European Journal of Medicinal Chemistry 221 (2021) 113566

Contents lists available at ScienceDirect

European Journal of Medicinal Chemistry

journal homepage: http://www.elsevier.com/locate/ejmech

New nimesulide derivatives with amide/sulfonamide moieties: Selective COX-2 inhibition and antitumor effects

Tuğba Güngör [a, *, 1], Adem Ozleyen [b, c, 1], Yakup Berkay Yılmaz [b, d], Pinar Siyah [e], Mehmet Ay [a], Serdar Durdağı [e], Tugba Boyunegmez Tumer [d, **]

[a] Department of Chemistry, Faculty of Sciences and Arts, Natural Products and Drug Research Laboratory, Çanakkale Onsekiz Mart University, Çanakkale, 17020, Turkey
[b] Graduate Program of Biomolecular Sciences, School of Graduate Studies, Canakkale Onsekiz Mart University, 17020, Çanakkale, Turkey
[c] School of Chemistry, University of Leicester, LE1 7RH, Leicester, United Kingdom
[d] Department of Molecular Biology and Genetics, Faculty of Arts and Science, Çanakkale Onsekiz Mart University, 17020, Çanakkale, Turkey
[e] Computational Biology and Molecular Simulations Laboratory, Department of Biophysics, School of Medicine, Bahçeşehir University, 34353, Istanbul, Turkey

ARTICLE INFO

Article history:
Received 27 March 2021
Received in revised form
15 May 2021
Accepted 18 May 2021
Available online 24 May 2021

Keywords:
Nimesulide
Synthesis
Amide
Sulfonamide
Anti-inflammatory
Anticancer
MD simulations
Docking
Binary QSAR models

ABSTRACT

Seventeen new amide/sulfonamide containing nimesulide derivatives were synthesized and characterized by several spectroscopic techniques and primarily investigated for their inhibitory potential on COX enzymes and other pro-inflammatory factors. Experimental analyses showed that among seventeen compounds, **N8** and **N10** have remarkable potency and selectivity for the COX-2 enzyme over COX-1 at very low doses as compared to nimesulide. Moreover, both **N8** and **N10** selectively reduced the Lipopolysaccharide (LPS)-stimulated COX-2 mRNA expression level while the COX-1 level remained stable. Both PGE_2 release and nitric oxide production in macrophage cells were significantly suppressed by the **N8** and **N10** treatment groups. *In silico* ADME/Tox, molecular docking and molecular dynamics (MD) simulations were also conducted. Additionally, all compounds were also screened in a panel of cancer cell lines for their antiproliferative properties by MTT and SRB assays. Compound **N17** exhibited a considerable antiproliferative effect on the colon (IC_{50}: 9.24 μM) and breast (IC_{50}: 11.35 μM) cancer cell lines. **N17** exposure for 48 h decreased expression of anti-apoptotic protein BCL-2 and increased the expression of apoptogenic BAX. Besides, the BAX/BCL-2 ratio was increased with visible ultrastructural changes and apoptotic bodies under scanning electron microscopy. In order to investigate the structural and dynamical properties of selected hits on the target structures, multiscale molecular modeling studies are also conducted. Our combined *in silico* and *in vitro* results suggest that **N8** and **N10** could be further developed as potential nonsteroidal anti-inflammatory drugs (NSAIDs), while cytotoxic **N17** might be studied as a potential lead compound that could be developed as an anticancer agent.

1. Introduction

Daily, over 30 million people with inflammatory symptoms are estimated to have a prescription for nonsteroidal anti-inflammatory drugs (NSAIDs) [1]. The primary action mechanism of NSAIDs is based on repressing the release of prostaglandins (PGs) and thromboxane (TxA) by inhibiting cyclooxygenase isoforms: COX-1 and COX-2. Unfortunately, long-term NSAID therapy leads to severe adverse effects in the GI-tract by undesired inhibition of COX-1 resulting in dramatic reductions in the gastroprotective PGs levels. COX-1 is the predominant isoform found in the different parts of the GI tract particularly mucosal epithelium of the gastric fundus, corpus, antrum, duodenum, jejunum, ileum, cecum, and colon [2]. Specifically, PG deficiency induced by NSAIDs cause gastric hypermotility due to inhibition of COX-1 but not COX-2 [3]. The highlighting of the risks of COX-1 inhibition has paved the way for the design of NSAIDs with COX-2 selectivity.

Selective COX-2 inhibition was thought to be a promising

* Corresponding author.
** Corresponding author.
E-mail addresses: tgungor@comu.edu.tr (T. Güngör), tumertb@comu.edu.tr (T.B. Tumer).
[1] T.G. and A.O. contributed equally.

https://doi.org/10.1016/j.ejmech.2021.113566
0223-5234/

strategy; the inhibition of inducible COX prevents the release of excess amounts of pro-inflammatory PGE_2 while spares the gastroprotective prostaglandin synthesis mediated by COX-1. In the beginning, the drugs with high selectivity towards COX-2 exhibited favorable safety profiles as compared to the traditional NSAIDs. Especially, the class of coxibs including celecoxib, etoricoxib, parecoxib, rofecoxib, valdecoxib, and lumiracoxib gained early success in clinics as selective COX-2 inhibitors. However, reports relevant to cardiovascular problems in rofecoxib, valdecoxib, and etoricoxib users brought about their withdrawal from markets. The underlying reason is said to be potential damage on the balance between COX-1 mediated prothrombotic TxA_2 and COX-2 mediated antithrombotic PGI_2 production [4]. Unlike other coxibs, celecoxib is still accessible in pharmacies with a warning label in its prescription highlighting the potential adverse actions.

4-NItro-2-phenoxyMEthane-SULphonanilIDE, NIMESULIDE (Scheme 1), has been in the markets for a long period as one of the most commonly used preferential anti-inflammatory agents with potent analgesic and antipyretic effects [5]. While coxibs are 375-800-fold more selective to COX-2, nimesulide has been shown to inhibit COX-2 about 21-folds more selectively than COX-1 [6]. In addition, it has been reported that at higher doses, its selectivity to COX-2 is lost [7]. For this reason, nimesulide does not lead to severe cardiovascular problems like other highly selective COX-2 inhibitors suppressing the biosynthesis of vascular prostacyclin. As well as it does not provoke gastric damage like other NSAIDs inhibiting gastroprotective PGs synthesis, even it is reported to be protective against NSAIDs-induced ulcers [8].

The most relevant adverse effect associated with nimesulide is hepatotoxicity. However, European Medicines Agency (EMA) confirmed that hepatic reactions caused by nimesulide are in line with other NSAIDs and generally relevant to the intake of high doses, which is far from those recommended [9,10]. A comprehensive and critical revision of clinical data regarding the efficacy and safety profile of nimesulide revealed that among other NSAIDs, it confers a favorable and unchanged benefit/risk assessment over time [11,12].

Apart from its distinctive safety properties, nimesulide has also unique therapeutic profiles that are not shared with other selective COX-2 inhibitors (Scheme 1). Nimesulide possesses a wide range of multitarget actions known to be important in the mitigation of inflammatory processes such as inhibition of reactive oxygen species (ROS), nitric oxide (NO), peroxynitrite ($ONOO^-$), cytokines, histamine, and elastase releases. It also downregulates the activities of nitric oxide synthase (NOS) and metalloproteinases (MMPs). Moreover, it reduces the rate of monocyte death, chemotaxis, and transendothelial migration [12]. Some *in vitro* and *in vivo* animal model studies demonstrated its inhibitory effects on cancer cell proliferation and metastasis [13]. Recently, nimesulide is recommended to be repurposed as a potential antidiabetic agent due to its anti-glycation activity [14]. Very recently, researchers suggested that nimesulide should be included in the list of the drugs to be tested for the identification of co-adjuvant in the treatment of COVID-19 [15]. They found that Nimesulide abolishes the transport function of the B0AT1-ACE-2 supercomplex for SARS-CoV-2 viral entry [15].

Multitarget pharmacological profiles represented by the chemical entity of nimesulide inspired us for the development of new derivatives with amide and sulfonamide moieties. For this purpose, new nimesulide derivatives (NDs) were designed, synthesized, and

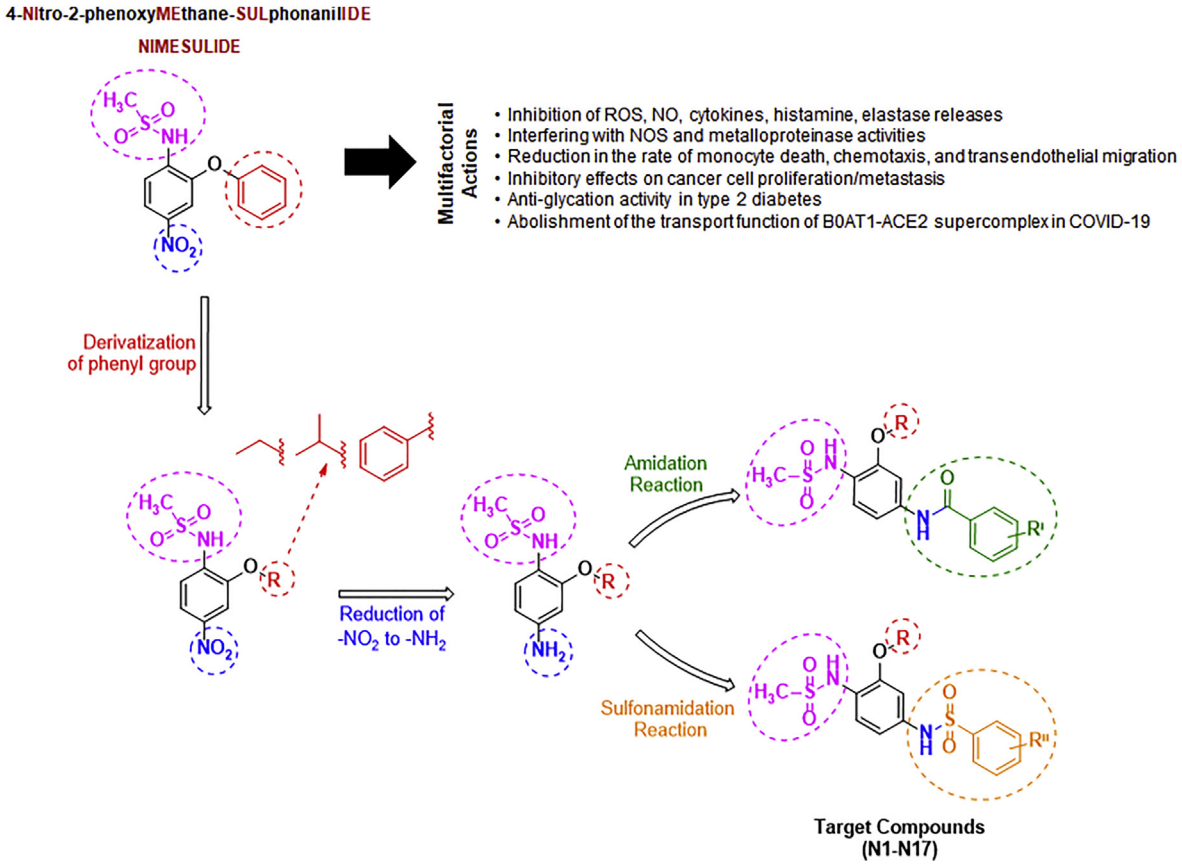

Scheme 1. Design process of new amide/sulfonamide derivatives of nimesulide as anti-inflammatory and anticancer agents.

investigated for their anti-inflammatory and anticancer effects. Moreover, *in silico* studies including molecular docking, molecular dynamics (MD) simulations, and ADME/Tox investigations were performed. Target compounds (**N1**−**N17**) were designed through three main steps (Scheme 1). In the first step, the phenyl group of nimesulide was changed with ethyl and isopropyl groups which are expected to be potentially active in the light of our preliminary theoretical studies (for compounds **N1-12** and **N14**−**16**). Also, the phenyl group was not changed in compounds **N13** and **N17**. The following step is the reduction of nitro to the amino group. The final step to form the target compounds **N1**−**N17** is amidation or sulfonamidation reactions between the amino group and benzoyl chloride/benzoic acid derivatives or benzenesulfonyl chloride derivatives bearing various functional groups (-NO_2, −F, −OCH_3, −$CONH_2$).

Nimesulide is the sole NSAID containing a nitro group. Although nitro-containing compounds are considered structurally unsafe molecules, there are many physiologically active therapeutics having this group in markets such as nilutamide, nitrendipine, nitrazepam, and nitromide. Indeed, the radical scavenger behavior of the nimesulide had been attributed to the incorporation of a 4-nitro group into the sulphoanilide structure [12]. Besides, the previous structure-activity (SAR) studies including new NDs reported that compounds without NO_2 possess lower antinociceptive activity. In our previous studies, a series of the nitro-containing benzamide compounds were synthesized and investigated for their anti-inflammatory and neuroinflammatory effects in lipopolysaccharide (LPS)-induced macrophages and microglia cells by focusing their inhibitory effects on pro-inflammatory factors, iNOS, COX-2, IL-1β, and TNF-α [16,17]. The promising results of nitro substituted benzamides encouraged us to expand the scope of these compounds. Thereupon, in the present study, the design of new compounds was executed by the combination of nimesulide and nitrobenzamides of our previous studies. Further, various functional groups (-F, −OCH_3, −$CONH_2$) instead of the nitro group and as well as sulfonamide moiety instead of amide were included in the product series to investigate the effects of different functional groups or pharmacophores on anti-inflammatory and anticancer activities.

2. Results and discussion

2.1. Chemistry

The synthetic strategy for seventeen new NDs (**N1**−**N17**) is outlined in Schemes 2 and 3. Ethoxy or isopropoxy derivatives of *N*-(4-amino-2-alkoxyphenyl)methanesulfonamides were synthesized in three steps (See Supporting Information). Firstly, 2-amino-5-nitrophenol was reacted with iodoethane or 2-iodopropane to obtain the etheric intermediates via Williamson ether synthesis [18−20]. The reaction of intermediates with methanesulfonyl chloride (MsCl) in the presence of sodium hydride at room temperature afforded dimethanesulfonamide derivatives which were subsequently converted into methanesulfonamide derivatives at basic hydrolysis conditions [18,19]. An alternative, one-step synthesis of methanesulfonamides was also performed using MsCl and pyridine at room temperature for 40 h in DCM with good yields (>80%) [21]. The nitro functionality was reduced with tin/hydrochloric acid to obtain amines in good yields (74 and 87%, ethyl ether and isopropyl ether derivatives, respectively) in the last step [22]. *N*-(4-amino-2-phenoxyphenyl)methanesulfonamide as the starting material of compounds **N13** and **N17** was synthesized beginning from 2-amino-5-nitrophenol according to the literature methods [22,23].

Final amide and sulfonamide products **N1-4**, **N6-11** and **N14**−**17** were synthesized in a convenient and mild approach by stirring *N*-(4-amino-2-alkoxyphenyl)methanesulfonamide derivatives and substituted benzoyl chlorides/benzenesulfonyl chlorides in the presence of triethylamine in chloroform at room temperature [22] (Scheme 2). While the reactions of amide derivatives **N1-4**, **N10**−**11** and **N16**−**17** were completed in short reaction times (2−3 h) with moderate to good yields (65−83%), the reactions of sulfonamide derivatives **N6-9** and **N14**−**15** were completed in longer reaction times (12−24 h) with 51−78% yields.

Additionally, amide products **N5**, **N12**, and **N13** were obtained in a different amidation way based on benzoic acid derivatives instead of benzoyl chlorides using coupling reagents such as DCC or EDCI.HCl (Scheme 3). The 16 h reaction of 2-nitro-4-methoxybenzoic acid and *N*-(4-amino-2-isopropoxyphenyl)methanesulfonamide with DCC in the presence of catalyst DMAP in DCM at reflux temperature gave the compound **N5** in 69% yield. In a similar way, compounds **N12** and **N13** were obtained at the reaction condition which is including terephthalamic acid (4-carbamoylbenzoic acid) as starting material in the presence of EDCI.HCl, HOBt and triethylamine in DMF at 100−120 °C for long reaction times (24 and 43 h, respectively).

Consequently, target nimesulide compounds **(N1**−**N17)** were synthesized successfully and identified by melting point, MS, FT-IR, ^{1}H and ^{13}C NMR spectroscopic techniques (See Experimental Part and Supporting Information). Also, the purity of compounds (>95%) was checked with HPLC analysis (See Experimental Part and Supporting Information). The structures of known starting materials were confirmed by the comparison with literature data. Model compound, *N*-(3-isopropoxy-4-(methylsulfonamido)phenyl)-4-methoxy-2-nitrobenzamide (**N5**) was confirmed by ^{1}H NMR as the presence of −NH singlet protons of amide and sulfonamide at 8.72 and 10.59 ppm. The doublet peak with 6H integration at 1.31 ppm, and the septet peak with 1H integration at 4.54 ppm corresponds to the −CH_3 and −CH protons of the isopropyl ether group, respectively. It was determined that the −CH_3 protons of sulfonamide and arylmethyl ether groups were resonated as singlet peaks with 3H integration at 2.89 ppm and 3.89 ppm, respectively. In addition, six aromatic protons were found in the range of 7.72−7.12 ppm. The evaluation of the ^{13}C NMR spectrum of compound **N5** showed carbonyl C=O signal at the highest chemical shift (164.07 ppm) and aromatic peaks of two phenyl rings in the range of 160.98−105.35 ppm. Also, aliphatic peaks were observed at the expected region of spectrum such as two isopropyl carbons at 22.02 and 70.56 ppm, methyl carbon of sulfonamide at 40.55 ppm and methyl carbon of arylmethyl ether at 56.78 ppm. FT-IR spectrum of **N5** showed the N−H stretching of amide and sulfonamide at 3319, 3246 cm^{-1} and the carbonyl stretching of amide at 1657 cm^{-1}. Also, aromatic C−H stretching at 3154-3068 cm^{-1}, aliphatic C−H stretching at 2980-2850 cm^{-1} and C−*O*−C stretching of ether at 1162 cm^{-1} were observed. The FT-IR, ^{1}H and ^{13}C NMR spectra of all other final products were determined almost in a similar pattern like compound **N5**. The MS of all new products showed the characteristic $[M-H]^-$ or $[M+H]^+$ molecular ion peaks to their corresponding molecular weight.

2.2. COX inhibition assay

NSAIDs exert their actions by inhibiting the activity of rate-limiting enzymes, COXs, in the pro-inflammatory prostanoids biosynthesis [24]. Retrospective studies stated that nonselective inhibition of COX might end up with undesirable side effects, particularly in the gastrointestinal system due to inhibition of the COX-1 enzyme [25]. Thus, preferential inhibition of the COX-2 enzyme has been pointed out as a safer therapeutic approach to healing inflammation-caused diseases. Firstly, the inhibitory effects

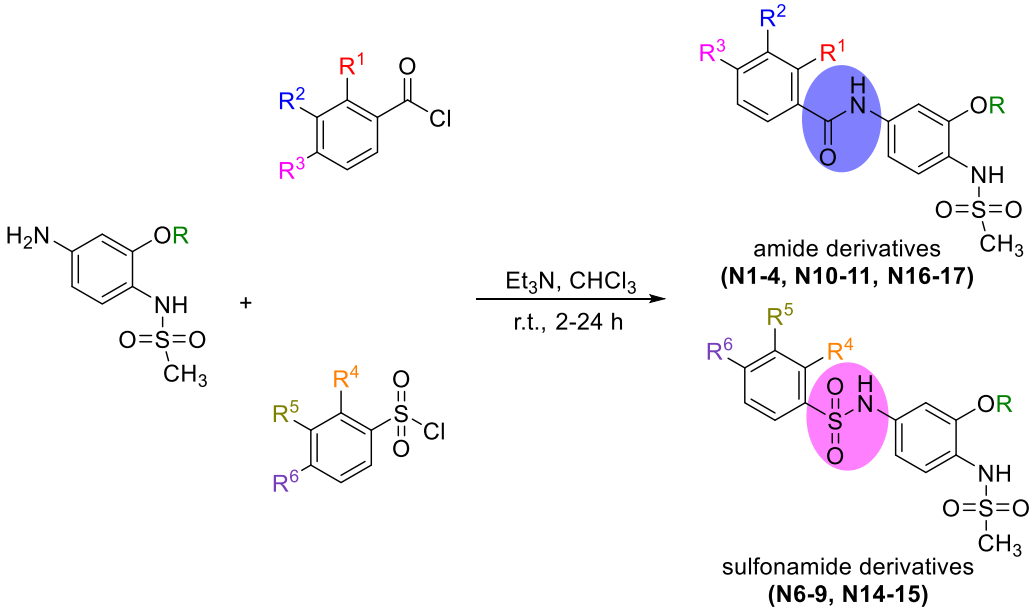

Comp.	R	R^1	R^2	R^3	Yield (%)
N1	Et	NO_2	H	H	65
N2	Et	H	NO_2	H	65
N3	Et	H	H	NO_2	71
N4	iPr	H	H	NO_2	73
N10	iPr	H	H	F	81
N11	iPr	H	H	OCH_3	75
N16	Et	H	H	F	83
N17	Ph	H	H	F	79

Comp.	R	R^4	R^5	R^6	Yield (%)
N6	Et	NO_2	H	H	75
N7	Et	H	NO_2	H	78
N8	Et	H	H	NO_2	70
N9	iPr	H	H	NO_2	55
N14	iPr	H	H	F	70
N15	iPr	H	H	OCH_3	51

Scheme 2. Synthesis of **N1-4**, **N6-11** and **N14**–**17** compounds.

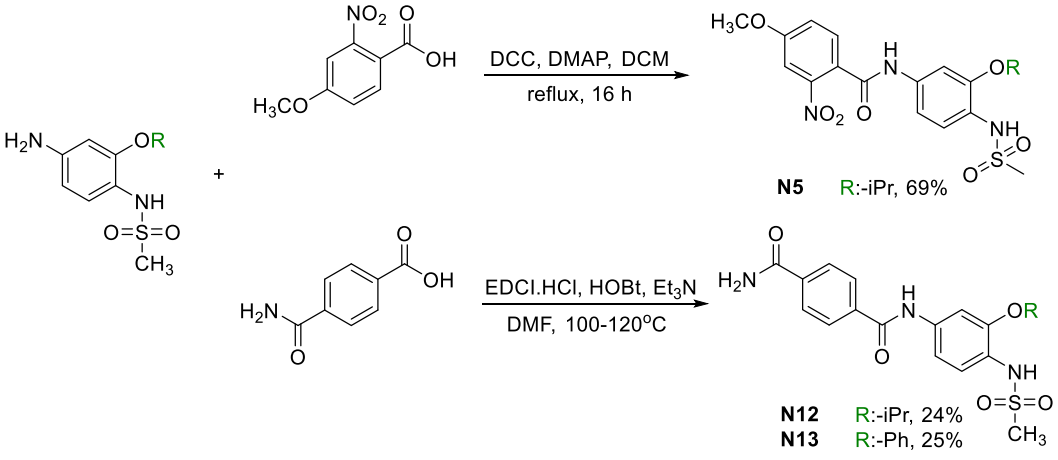

Scheme 3. Synthesis of **N5**, **N12** and **N13** compounds.

of seventeen NDs were investigated on the COX-2 enzyme at 1 μM dose. The results were illustrated as a percentage of remaining enzyme activity in Fig. 1. Among the seventeen compounds, **N1**, **N2**, **N3**, **N4**, and **N6** showed similar or better inhibitory effects as compared to reference compound nimesulide, however, the best inhibitory scores were obtained for **N8** and **N10** with 88.0 and 72.8%, respectively (Fig. 1A). As shown in Fig. 1B, the compounds with inhibitory effect on COX-2 were also analyzed on the recombinant COX-1 enzyme at 10 μM dose. According to results, only **N8** and **N10** decreased the activity of the COX-1 enzyme by 21.0 and 27.2%, respectively. However, at identical doses, reference compound nimesulide exhibited no inhibitory effect on the enzymatic activity of COX-1, it decreased the COX-2 activity by 12.1%. The findings for **N8** and **N10** in terms of both enzymes were highly compatible with the effects of celecoxib (Fig. 1B). According to the results, **N8** and **N10** compounds were selected as lead anti-inflammatory compounds and decided to be analyzed further through cell-based assays.

2.3. PGE_2 release from LPS induced THP-1 cells and COX-1/COX-2 expression levels

THP-1 human monocytic cell line is a good model to investigate the anti-inflammatory effects of the compounds. When they are challenged with PMA stimulation, they differentiate into adherent LPS inducible cells with macrophage-like phenotypes (Fig. 2A). PGE_2 production can be stimulated in response to inflammation in various diseases through activated arachidonic acid metabolism [26]. PGE_2 mediates the inflammatory cascades and excessive PGE_2 production demonstrates the pathophysiological process in organisms especially in the kidney [27]. Thus, suppression of PGE_2 release is important for the prevention and treatment of inflammation. In the present study, 50 and 100 μM doses of **N8** suppressed the release of PGE_2 by 77% and 44%, and **N10** suppressed the production of PGE_2 by 67% and 68%, respectively (Fig. 2B).

Additionally, 50 and 100 μM doses of **N8** suppressed the COX-2 mRNA expressions 47% and 60% in 1 μg/mL LPS-induced THP-1 macrophages, respectively. At the same doses, **N10** downregulated the COX-2 mRNA expressions by 53% and 61%, respectively. Suppression on COX-2 levels for both compounds was found to almost as effective as positive control celecoxib. Furthermore, both compounds did not change the COX-1 mRNA expressions significantly (Fig. 2C). These results suggested that **N8** and **N10** preferentially suppressed COX-2 mRNA levels without affecting COX-1 levels significantly similar to celecoxib.

2.4. Screening of pro-inflammatory markers

The primary pharmacological action of nimesulide is based on preferential inhibition of COX-2 thus the production of prostaglandins particularly, PGE_2. However, it takes the strength as an effective anti-inflammatory drug from its suppressive effects on other pro-inflammatory factors such as NO/iNOS signaling and cytokines. *In vitro* and *in vivo* studies reported that nimesulide at

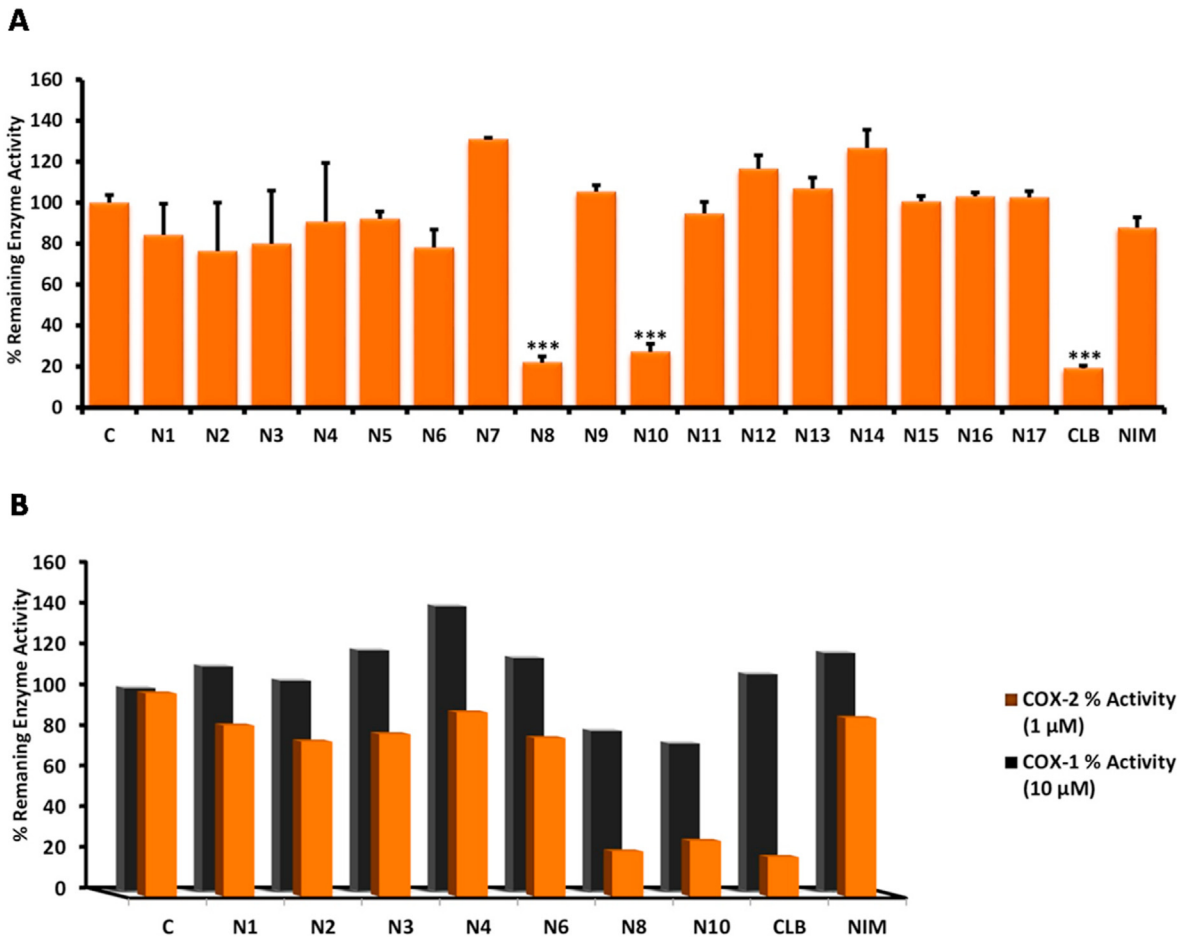

Fig. 1. Inhibitory effects of NDs on recombinant COX-2 enzyme at 1 μM (A, B, orange bars) and effective compounds were also screened on COX-1 enzyme at 10 μM (B, black bars). As positive control nimesulide and celecoxib were examined at same doses. C: Control. *p < 0.02, **p < 0.005, ***p < 0.001.

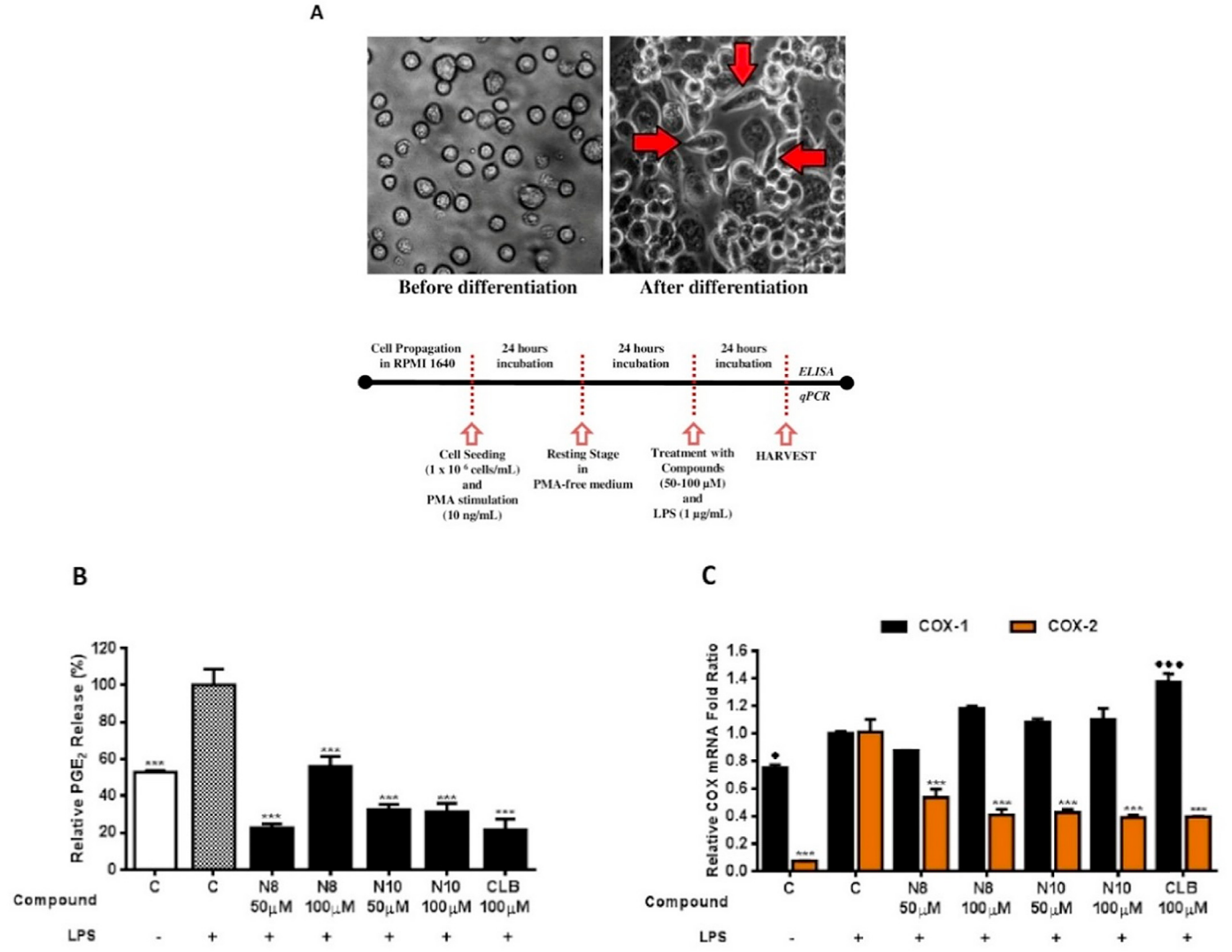

Fig. 2. Morphological changes of THP-1 cells were imaged before and after PMA treatment by using inverted microscope (A). The effects of **N8** and **N10** on PGE_2 release (B) and mRNA expression of COXs in activated THP-1 (C) at 50 and 100 μM doses. Celecoxib (100 μM): Positive control. C: Control. *p < 0.02, **p < 0.005, ***p < 0.001.

pharmacological concentration effectively inhibits NO release and production of TNFα [28,29]. Previously, Bogaart et al. reported that for NO production PMA-differentiated THP-1 did not give a response to LPS stimulation while murine macrophages such as RAW264.7 cell line could be triggered [30]. Bertholet et al. stated that NO might be released by murine macrophages in response to cytokine activation but not by human macrophages under the same conditions, even though iNOS is expressed at both mRNA and protein levels [31]. Our previous results also support these findings [32]. The reason behind this issue is still controversial but it is thought to be a lack of complete mechanism required for NO synthesis in the THP-1 cellular environment and epigenetic regulations around the iNOS transcription start site [31,33]. However, Knowles and Moncada reported 81–93% similarity in NOS genes between mammalian orthologs and further computational analyses revealed a high degree of three-dimensional overlap between the oxygenase domains of human and murine iNOS enzymes [34–37]. This observation demonstrates the potential utility of the cell-based murine iNOS assay to identify inhibitors of the human enzyme. For this reason, in the current study, to screen the effects of **N8** and **N10** on LPS induced NO/iNOS signaling and pro-inflammatory cytokine expression, the RAW264.7 cell line was used. Accordingly, murine macrophages were stimulated with 1 μg/mL LPS treatment in the presence and absence of compounds. As compared to the LPS-free group, LPS stimulation triggered the NO production in cells (Fig. 3A). Compound **N8** decreased the NO release at 20 and 50 μM doses by 40.7 and 68.1%, respectively. On the other hand, 20 and 50 μM doses of **N10** reduced the NO release by 43.1 and 46.4%, respectively. In contrast to **N8** and **N10**, reference compound nimesulide at 20 μM slightly increased the NO production as compared to the control but the differences were not found to be statistically significant. In the assay, 1400 W was used as a positive control, which is a very potent and selective iNOS inhibitor, and at 20 μM it decreased the NO release by 62.5%. Besides, the effects of **N8** and **N10** on the expression level of LPS-induced iNOS expression in murine macrophages were determined by qPCR analysis. As shown in Fig. 3B, the expression level of iNOS at the mRNA level remained stable in the **N8** treated group as compared to the control group, however, the iNOS expression was decreased by the **N10** treatment in a dose-dependent manner. **N10** down-regulated the expression by 40% at 20 μM dose and almost completely suppressed at 50 μM dose.

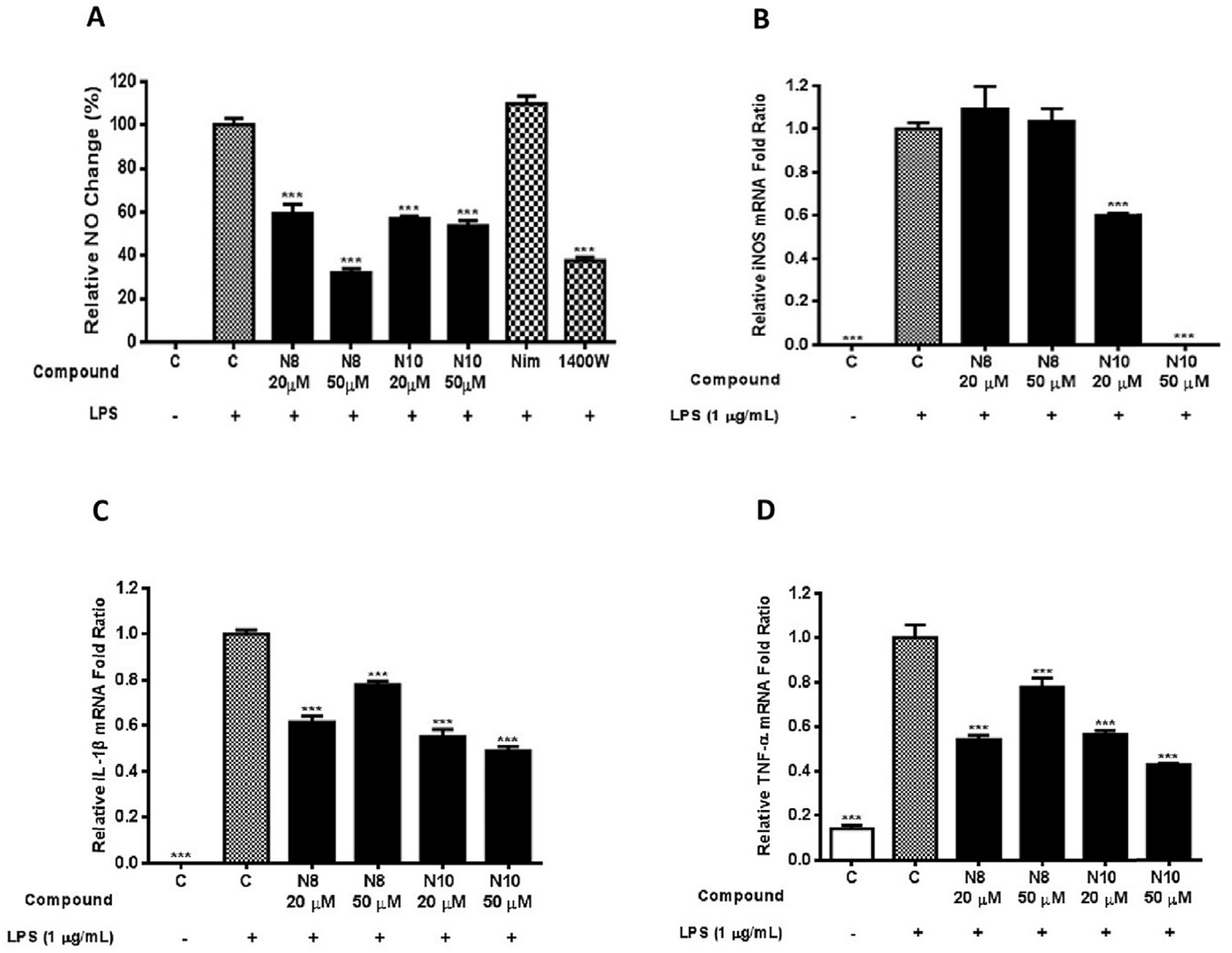

Fig. 3. The effects of **N8** and **N10** on NO production in LPS-treated murine RAW 264.7 cells (A). The effects of **N8** and **N10** on mRNA expression of iNOS (B), IL-1β (C), and TNF-α (D). Nimesulide (20 μM): Reference compound. 1400 W (20 μM): Positive control. C: Control. ***$p < 0.001$.

Overexpression of pro-inflammatory markers including IL-1β and TNF-α is associated with the release of exaggerated amounts of cytokines that lead to the progression of several inflammatory diseases such as metabolic syndrome, cancer, type II diabetes, and Alzheimer's disease [38]. In this study, 20 and 50 μM doses of **N8** led to a reduction in the mRNA expression level of IL-1β by 39 and 22%, respectively. Additionally, at the same doses, **N10** reduced the IL-1β mRNA level by 45 and 51% as compared to the control group (Fig. 3C). The expression of TNF-α was also changed by **N8** and **N10** treatment at 20 and 50 μM doses. The treatment of **N8** down-regulated the mRNA expressions of TNF-α by 46 and 22%, respectively. Additionally, **N10** reduced the LPS-induced TNF-α mRNA level by 44 and 57% at the same doses (Fig. 3D).

2.5. Anticancer properties of compounds N1–N17

The synthesized compounds were screened *in vitro* for their antiproliferative activity against three different human cancer cell lines: MCF-7 (breast carcinoma), PC-3 (prostate carcinoma) and HT-29 (colon carcinoma). Human umbilical vein endothelial cells (HUVEC) were used as non-cancerous control cells to represent the selectivity of the compounds for cancerous tissues. We determined the cytotoxicity of the compounds in two successive steps: 1) Screening of all the compounds at 100 μM by MTT assay. 2) Evaluating the IC_{50} values of the compounds which resulted in more than 50% inhibition at the first step, by SRB assay. Accordingly, screening studies resulted in a single effective cytotoxic compound, the remaining cell viabilities in **N17**-treated breast, colon, and prostate cancer cell lines were determined as 22, 33, and 25%, respectively. These results were found highly compatible with the effects of positive control doxorubicin for which cell viabilities remained at 14, 21, and 12%, in the same cell lines (Table 1).

Therefore, **N17** was selected for the determination of the half-maximal inhibitory concentration (IC_{50}) values by performing the SRB assay. For this purpose, those cells were treated with **N17** at different final concentrations (0–200 μM) for 48 h. As evident from Table 2, the IC_{50} values of **N17** were found as 9.24 and 11.35 μM in the colon and breast cancer cell lines, respectively. However, the value was higher than 100 μM in prostate cancer cells. To display the selective cytotoxic characteristic, **N17** was also evaluated in healthy cells, and its IC_{50} value was determined higher than 200 μM.

Apart from the cytotoxic properties of **N17**, its effects on the long-term survival and ability of the cells to form colonies were also

Table 1
Cytotoxicities of NDs in MCF-7, HT-29, and PC-3 cell lines at 100 μM concentration. Percentage cell viability was presented as the mean ± SD of three independent experiments.

Compound (100 μM)	Cell viability (%)		
	MCF-7	HT-29	PC-3
Vehicle	100.0 ± 17.3	100.0 ± 15.6	100.0 ± 6.7
N1	122.0 ± 4.6	111.5 ± 27.4	100.5 ± 5.8
N2	90.8 ± 14.2	70.4 ± 19.7	90.2 ± 11.1
N3	115.7 ± 26.2	114.0 ± 29.7	84.8 ± 11.6
N4	100.8 ± 20.1	124.3 ± 40.0	81.0 ± 11.2
N5	63.5 ± 6.7	110.6 ± 19.6	94.2 ± 10.7
N6	138.7 ± 21.4	133.4 ± 19.9	77.9 ± 11.9
N7	127.0 ± 24.5	115.8 ± 20.8	75.5 ± 10.6
N8	118.7 ± 22.1	118.4 ± 21.6	65.7 ± 27.6
N9	57.9 ± 6.4	75.4 ± 12.9	91.4 ± 12.9
N10	109.7 ± 15.2	49.6 ± 24.0	79.4 ± 12.9
N11	152.8 ± 11.6	67.9 ± 7.3	65.8 ± 5.0
N12	61.9 ± 8.3	79.4 ± 14.8	49.8 ± 10.9
N13	53.1 ± 8.6	64.4 ± 17.8	88.7 ± 16.3
N14	130.4 ± 29.7	92.9 ± 28.4	75.5 ± 7.3
N15	130.8 ± 26.5	101.6 ± 26.9	68.6 ± 22.7
N16	64.4 ± 7.3	80.1 ± 6.0	90.0 ± 9.7
N17	**22.2 ± 3.0**	**33.1 ± 3.8**	**24.8 ± 6.6**
Doxorubicin	14.1 ± 3.8	21.0 ± 5.1	11.8 ± 0.9

Table 2
IC_{50} values of DOX and **N17** in the HT-29 colon cancer, PC-3 prostate cancer, MCF-7 breast cancer, and HUVEC healthy cell lines. The values are expressed as the mean ± SE of three independent experiments.

Compound (μM)	HT-29	PC-3	MCF-7	HUVEC
Doxorubicin	0.15 ± 0.06	16.86 ± 1.19	0.16 ± 0.08	0.10 ± 0.04
N17	9.24 ± 1.71	>100	11.35 ± 1.55	>200

determined by clonogenic assay in a dose-dependent manner. As shown in Fig. 4, the treatment of **N17** led to a dose-dependent decrease in the colony number of breast cancer cells. Even, it was not seen any colony formation in the highest concentration of **N17**.

To elucidate the mechanism lying behind the antitumor effects of **N17** partially, we investigated the expression of apoptosis-related proteins BAX (BCL-2-associated X protein) and BCL-2 (B-cell lymphoma 2) by Western blot analyses. According to the results, the expression of pro-apoptotic BAX protein was up-regulated by 24 h **N17** treatment in a dose-dependent manner. Besides, the level of anti-apoptotic BCL-2 was significantly down-regulated in the same treatment group. The increasing ratio of BAX/BCL-2 shown in Fig. 5 suggested that **N17** may lead to apoptotic cell death by the activation of intrinsic pathway.

To confirm the apoptotic effects of **N17**, the apoptotic bodies and ultrastructural changes in cancer cells were examined by SEM analyses. As marked with red arrows, the treated cells appeared to have irregular shapes and exhibited apoptotic structures including an increasing number of blebs and apoptotic bodies as compared to the control cells. While the control cells conserved their typical morphologies with quite adherent appearance, **N17**-treated cells lost their pre-apoptotic structures by elongating and shrinkage (Fig. 6).

2.6. Hybrid in silico studies

The synthesized molecules (**N1**–**N17**) were targeted to human COX-1 and COX-2 target proteins. The interactions occurred between the ligands and the crucial amino acid residues at the target proteins were determined by *in silico* simulations. The pharmacokinetics (absorption, distribution, metabolism and excretion (ADME)) characteristics of the synthesized molecules were also determined. The toxicities that molecules could cause were also estimated. The therapeutic activities against various diseases were investigated.

2.6.1. Molecular docking studies

After ligand and protein preparation, grid boxes were generated from the ligands at the binding pockets of the target proteins. The ligands (**N1**–**N17**) were docked into these grid boxes of human

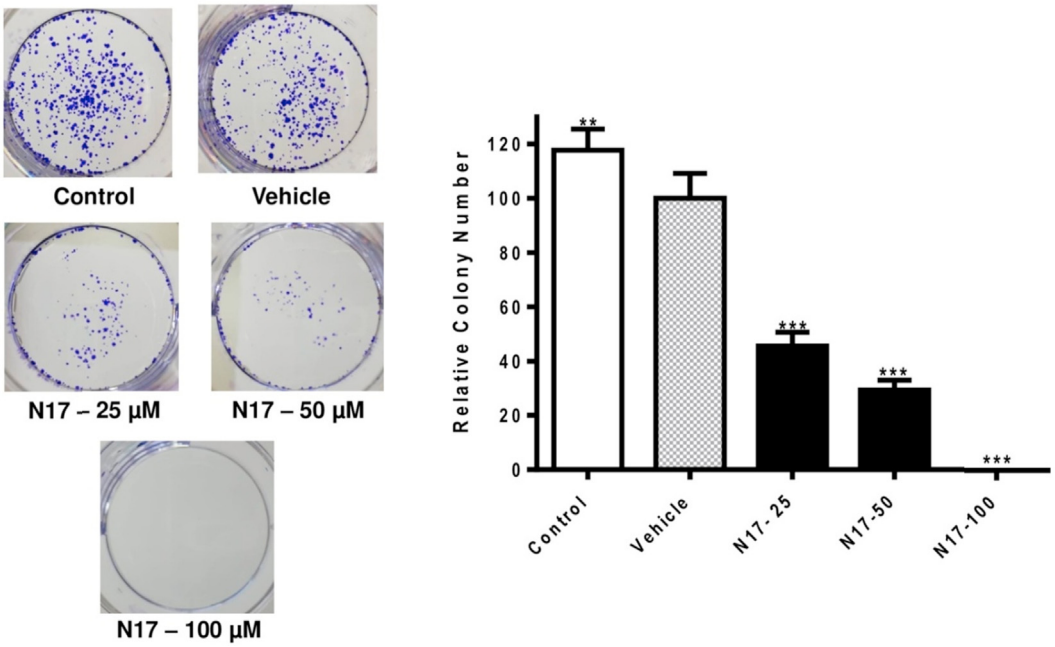

Fig. 4. The effect of **N17** on colony formation ability of MCF-7 cancer cells. Cells were treated with 10 and 25 μM of the compound **N17**. ***p < 0.001.

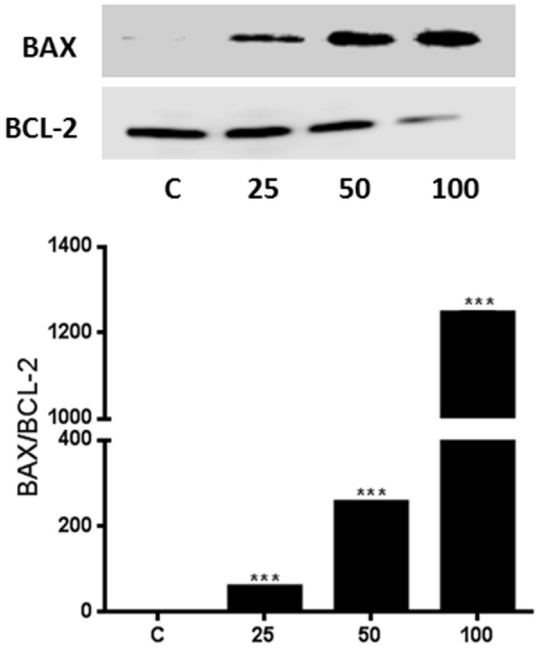

Fig. 5. The effects of **N17** on BAX/BCL-2 expression levels in MCF-7 breast cancer cells. Cells were treated with 10 and 25 μM of the compound **N17** for 24 h. C: Control.***$p < 0.001$.

COX-1 and COX-2 proteins to estimate their binding energies and binding poses. All molecular docking studies were performed by a grid-based docking program (Glide) [39]. Tables 3 and 4 show the scores of top-docking poses of the studied compounds and reference molecules (i.e., known inhibitors of studied targets). Results show that some of the compounds do not form binding poses or have low docking scores in COX-1 (Table 3). The obstacle in targeting all these ligands to COX-1 while they form strong binding to the COX-2 protein may represent target-specific inhibition of COX-2 by these compounds. In addition, the fact that nimesulide gives better binding scores to COX-2 than to COX-1 protein confirms both *in silico* and *in vitro* results [23,40].

Apoptosis in a cell is governed by pro-apoptotic and anti-apoptotic proteins of the BCL-2 family. When BCL-2 family get unbalanced, it can prevent the cells from undergoing apoptosis and cause tumor growth. BCL-2 is overexpressed in many human cancer types and has often been associated with the increase in tumor development and resistance to cancer treatment. Thus, BCL-2 protein is one of the key targets for cancer treatment [41–43]. Most of the compounds studied showed higher docking scores against the BCL-2 protein (Table 3) compared to the FDA-approved BCL-2 inhibitor Venetoclax (Table 4). This could indicate that these molecules could be promising inhibitors for the BCL-2 target.

2.6.2. *Interactions between studied target proteins and hit molecules investigated by MD simulations*

Interactions between COX-1, COX-2 and BCL-2 target proteins and synthesized compounds were investigated throughout the MD simulations. Compounds that show successful docking poses at the target proteins were used in MD simulations. For this aim, top-docking poses were used. Simulations were run at 310 K for 100 ns in the Desmond program [44]. MM/GBSA analyses were conducted for the assessment of the average binding free energies of the compounds at the binding sites of the targets. Fig. 7 shows 2D ligand (**N10**) interactions diagrams, residue interaction fractions and **N10**-COX-1 residue contact maps during the simulations. Results show that especially Val349, Tyr385, Ser530, and Leu531 have crucial interactions for the ligand binding, and they mainly

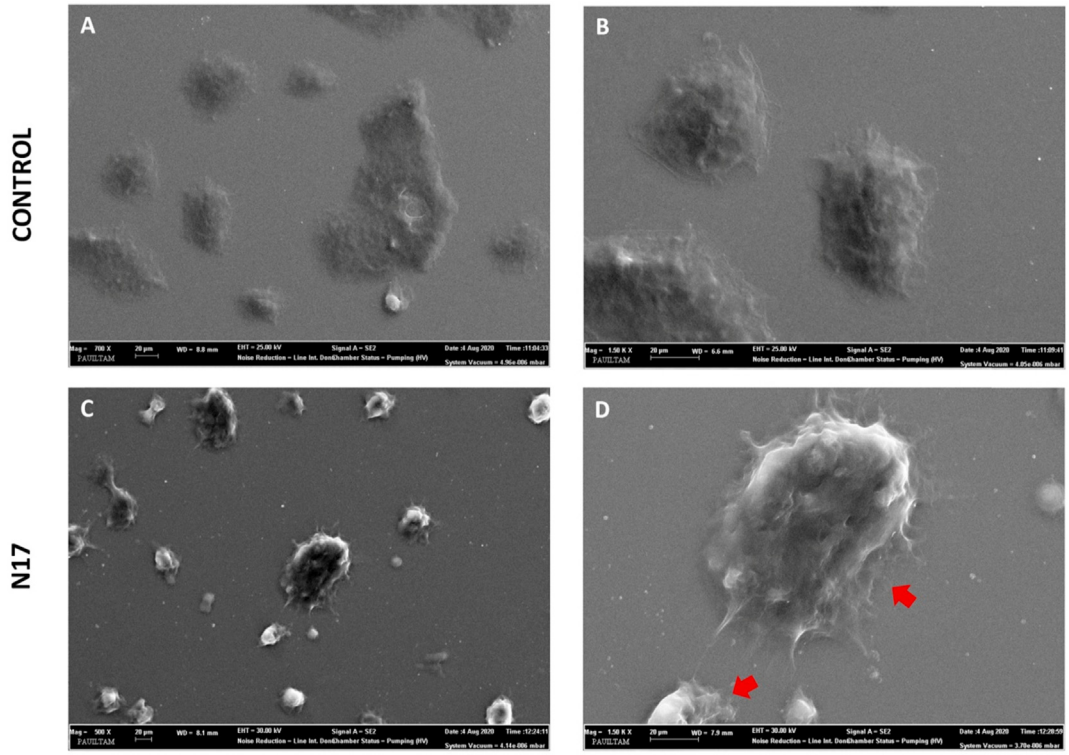

Fig. 6. The ultrastructural changes of treated colon cancer cells were displayed by SEM analyses. The treatment of **N17** (C,D) for 48 h led to the loss of normal morphology and normal cell size as compared to the untreated cells (A,B). Magnifications: 700x for A; 750x for C; 1,500x for B, D micrographs.

Table 3
Molecular docking scores of the compounds against COX-1, COX-2, and BCL-2 targets.

Compound	COX-1 docking score (kcal/mol)	COX-2 docking score (kcal/mol)	BCL-2 docking score (kcal/mol)
N1	–	–	−6.255
N2	−5.593	−4.041	−5.176
N3	–	–	−5.072
N4	–	–	−5.199
N5	–	–	−4.701
N6	–	−5.725	−5.643
N7	–	−5.740	−5.365
N8	–	−5.565	−6.412
N9	–	−5.580	−6.111
N10	−5.397	−3.406	−4.878
N11	–	–	−5.306
N12	–	–	−5.682
N13	−2.472	−6.447	−6.798
N14	–	–	−5.380
N15	–	−5.287	−6.171
N16	−4.869	–	−6.033
N17	–	−8.648	−6.420

Table 4
Molecular docking scores of the reference molecules against COX-1, COX-2, and BCL-2 targets.

Reference Molecules Docking Scores (kcal/mol)		
COX-1	Celecoxib	−4.255
	Nimesulide	−3.641
COX-2	Rofecoxib	−9.742
	Nimesulide	−8.014
BCL-2	Venetoclax	−4.770
	Nimesulide	−5.594

maintain their contacts with the **N10**. Hydrophobic interactions occur with Val116, Val349, Tyr355, Ala527, Leu531 amino acids while hydrogen bonds are established with Tyr385, Ser530 amino acids, and water bridges are formed with Tyr348, Tyr355, Tyr385 amino acid residues.

Fig. 8 shows 2D ligand interactions diagram, residue interaction fractions and COX-2 residue contact maps during the simulations for **N8**. MD results show that especially Val116, Arg120, Leu352, Leu359, Arg513, Phe518, and Val523 form crucial interactions with the **N8**. Hydrogen bonds are established with Ser353, Ser359, and Ser530 residues while hydrophobic interactions occur at Val349, Tyr355, Leu359, Leu531, and Leu534 amino acids at the binding site. In addition, water bridges are formed with Leu352, Tyr355, Tyr385, and Ser530.

Fig. 9 shows ligand interactions diagram, residue interaction fractions and BCL-2 residue contact maps during the simulations for **N17**. Simulation results show that especially Phe101, Asp108, Phe109, Met112, Gln115, Leu134, and Arg143 at the BCL-2 binding site construct critical interactions with the **N17** and these interactions maintain throughout the simulations. Hydrogen bonds are formed with Asp108 and Gln115 residues. Furthermore, hydrophobic interactions occurred with Phe101, Phe109, Met112, Leu134, and Arg143 and water bridges are formed with Asp108 and Glu111.

Table 5 shows average Molecular Mechanics/Generalized Born Surface Area (MM/GBSA) results for the selected compounds at three different targets. In order to compare the binding free energy results, same MD simulations protocols were also conducted for known inhibitors of studied targets. Reference complex structures were used directly from their co-crystallized forms. The known ligands Celecoxib, Rofecoxib and Venetoclax that were co-crystallized with the protein were kept in their targets COX-1 (6Y3C), COX-2 (5KIR) and BCL-2 (4LXD), respectively. These target proteins were prepared, and MD simulations were performed. All simulation protocols were conducted in the same way using the same settings as the other studied ligand-protein complex systems in this study.

Average MM/GBSA scores of Celecoxib, Rofecoxib and Venetoclax were found as −72.58, −65.56, and −81.85 kcal/mol, respectively. While average MM/GBSA results of selected hit ligands and reference compounds have similar binding free energy results, MM/GBSA score of Venetoclax was found higher compared to hit compounds. The reason could be different molecular sizes of the hits and Venetoclax. Molecular weight of Venetoclax (868.4 g/mol) is much higher than studied compounds. Moreover, Nimesulide was used as the reference compound and its average MM/GBSA scores were found as −53.62 and −36.39 kcal/mol for COX-2 and BCL-2 proteins, respectively. The MM/GBSA results of the hit molecules were compared with the values given by the reference molecules and it was determined that they were in an acceptable range (Tables 5 and 6). The results of reference compounds were considered, and molecules with similar or higher docking and MM/GBSA scores were selected. As a result, **N2** and **N10** at COX-1; **N6**, **N7**, **N8**, **N9**, **N13**, and **N17** at COX-2; **N8**, **N10**, **N13**, and **N17** at BCL-2 showed higher interaction energy scores (in absolute values) compared to other compounds.

2.6.3. Pharmacokinetic properties, toxicity and disease-QSAR analysis of the molecules

The pharmacokinetic characteristics, toxicity properties, metabolites and therapeutic activities of the molecules were predicted by MetaCore/MetaDrug platform which is an integrated software suite of Clarivate Analytics (https://portal.genego.com/). 25 common diseases and 26 different toxicity quantitative structure-activity relationships (QSAR) models were used in the analysis of synthesized compounds (Table 7).

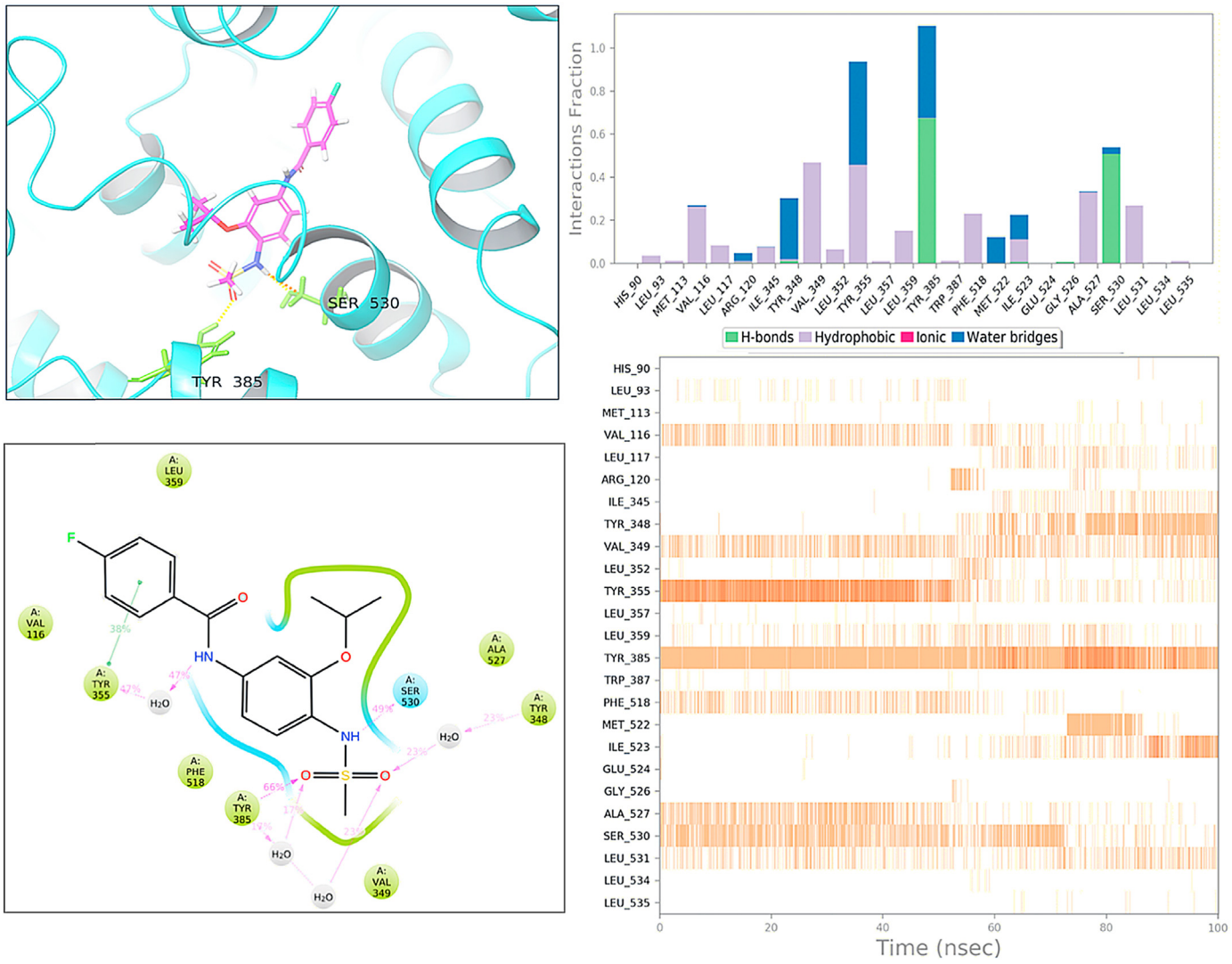

Fig. 7. 2D and 3D ligand interactions diagrams, interaction fractions and contact map of **N10** at the binding pocket residues of COX-1.

All compounds were screened at the inflammation-QSAR model. The used inflammation disease-QSAR model (Training set N = 598, test set N = 93) has following statistical results: Sensitivity = 0.86, Specificity = 0.84, Accuracy = 0.85, MCC = 0.69.

Compounds **N6**, **N7**, **N8**, **N9**, **N10**, **N15**, **N16** and **N17** showed activity prediction against inflammation in binary QSAR models (Table 7). It was also determined that all molecules obey the druggability rules and can be promising drug candidates for the future (Supporting Information, Table S2).

Precited therapeutic activity values of compounds against cancer were screened using the binary QSAR models. The used cancer disease-QSAR model (Training set N = 886, test set N = 167) has following statistical results: sensitivity = 0.89, specificity = 0.83, accuracy = 0.86, MCC = 0.72.

Molecules with predicted therapeutic activity values higher than 0.5 were identified as molecules with therapeutic activity potential. Accordingly, it is predicted that **N6**, **N7**, **N8**, **N9**, **N12**, **N13**, **N14** and **N15** molecules may have anti-cancer effects (Table 8). The fact that these molecules were found to target the BCL-2 protein (Table 3), which is often associated with cancer, was also confirmed by the prediction of cancer therapeutic activities of the molecules in QSAR studies.

2.7. Structure activity relationship

According to the anti-inflammatory and anticancer studies of NDs, the preliminary structure activity relationship (SAR) was characterized (Fig. 10). It was determined that compound **N8**, *N*-(3-ethoxy-4-(methylsulfonamido)phenyl)-4-nitrobenzenesulfonamide and compound **N10**, *N*-(3-isopropoxy-4-(methylsulfonamido)phenyl)-4-fluorobenzamide were showed better COX-2 inhibition (88.0 and 72.8%, respectively) than nimesulide and compatible with celecoxib. **N8** and **N10** decreased the activity of COX-1 enzyme (21.0 and 27.2%, respectively) but their selectivity scores were still better than nimesulide. Likewise, compound **N8** and **N10** suppressed the COX-2 mRNA expressions in LPS-induced THP-1 macrophages (47 and 53% for 50 μM doses, 60 and 61% for 100 μM doses, respectively). Furthermore, it was observed that compound **N8** and **N10** suppressed the release of PGE_2 and NO, effectively. When the other compounds were evaluated in detail, nitro containing amide derivatives named as **N1**–**N4** and 2-nitrophenylsulfonamide derivative **N6** showed similar or better inhibitory effect as compared to the standard compound, nimesulide. Unlike, compound **N7** (3-nitrosubstituted sulfonamide derivative) and compound **N9** (isopropyl ether

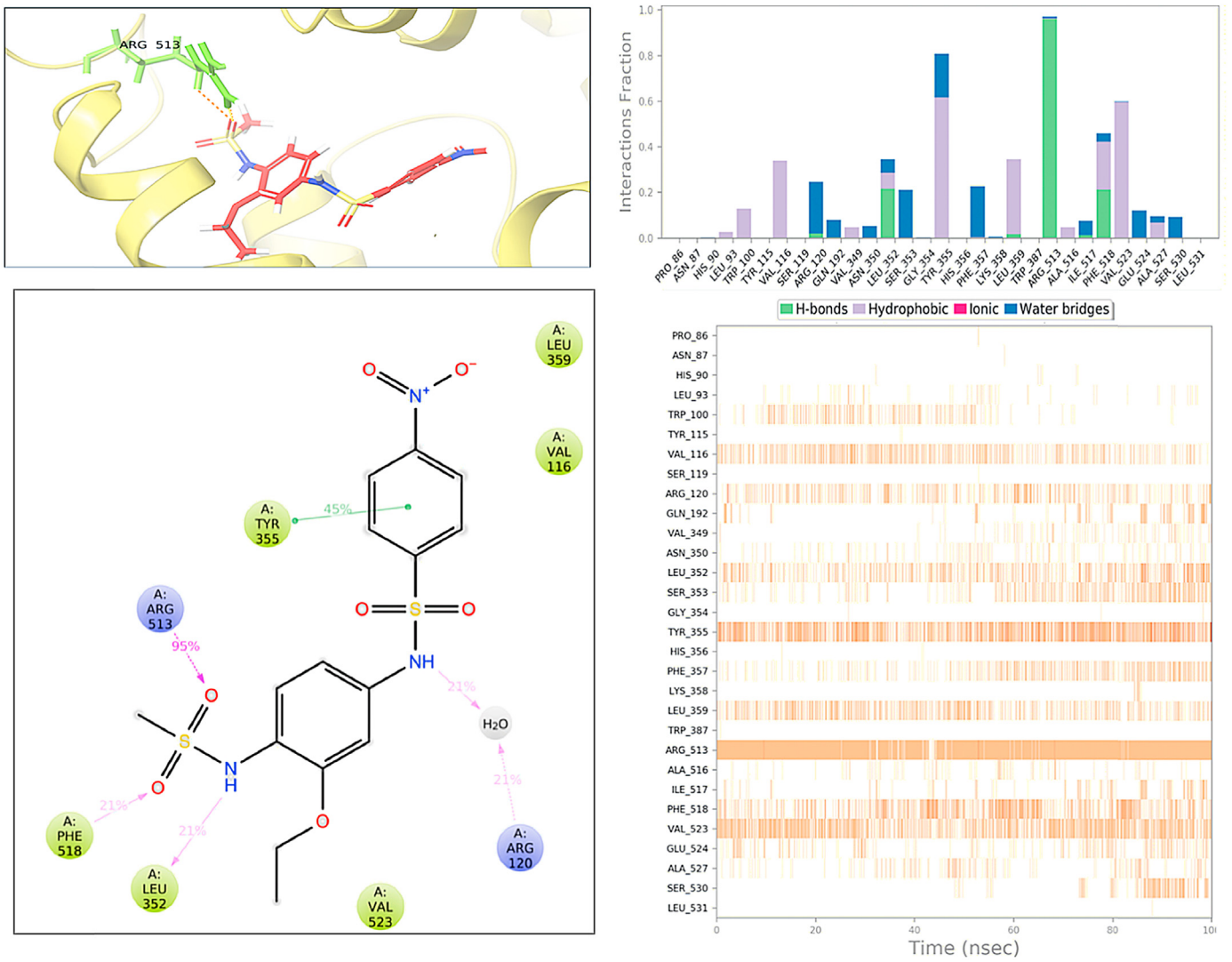

Fig. 8. 2D and 3D ligand interactions diagrams, interaction fractions and contact map of **N8** at the binding pocket residues of COX-2.

derivative) which are structurally very similar to **N8** did not show significant COX-2 inhibitory activity. So, it can be concluded that among the nitro containing amide and sulfonamide derivatives **(N1**−**N9)**, the effective compound must have nitro group at the 4-position of the phenyl ring, must be ethyl ether derivative and must connect the two phenyl rings with sulfonamide bridge to show good anti-inflammatory effect. Among the nitro-free and −F, $-OCH_3$, $-CONH_2$ containing amide and sulfonamide derivatives **(N10**−**N17)**, while isopropoxy bearing 4-fluorobenzamide compound **(N10)** showed good anti-inflammatory effects, compounds **N14** (sulfonamide derivative), **N16** (ethoxy derivative) and **N17** (phenoxy derivative) did not show meaningful COX-2 inhibitory activity. The positive effect of groups (-OCH_3, $-CONH_2$) except fluorine at 4- position of phenyl ring was not determined.

When anticancer results of compounds **N1**−**N17** were evaluated, *N*-(3-phenoxy-4-(methylsulfonamido)phenyl)-4-fluorobenzamide (**N17)** was found to be most active antiproliferative compound on HT-29 colon cancer cells (IC_{50}: 9.24 μM) and on MCF-7 breast cancer cells (IC_{50}: 11.35 μM) with minimal effect on healthy cells. In addition, compounds **N2**, **N11** and **N13** for colon cancer, compounds **N8, N11, N12** and **N15** for prostate cancer, compounds **N5**, **N9, N12**, **N13** and **N16** for breast cancer showed moderate cytotoxic effects. Also, it was observed that there was no correlation between COX inhibition and anticancer results due to compounds showing high COX-2 inhibitory activity-**N8** and **N10** were not the most active antitumor agents. However, it can be said that compound **N10** decreased the viability of colon cancer cells to some extent (49.6%).

3. Conclusions

In this study, a series of new amide/sulfonamide NDs **(N1**−**N17)** were synthesized, characterized, and evaluated for their ability to inhibit COX enzymes/several pro-inflammatory factors and for their antiproliferative effects on different cancer cell lines. Accordingly, among seventeen compounds, **N8** as a nitro containing sulfonamide and **N10** as a nitro-free amide derivative demonstrated a highly potent and relatively selective inhibitory effect on COX-2 enzyme with anti-inflammatory potential as evidenced by cell-free and cell-based *in vitro* studies. At the same time, **N8** and **N10** were not cytotoxic neither in three different cancer cell lines nor in normal endothelial cells at their active concentrations, therefore, they could be further optimized and explored as potentially safe lead molecules. For cytotoxicity evaluations, among all

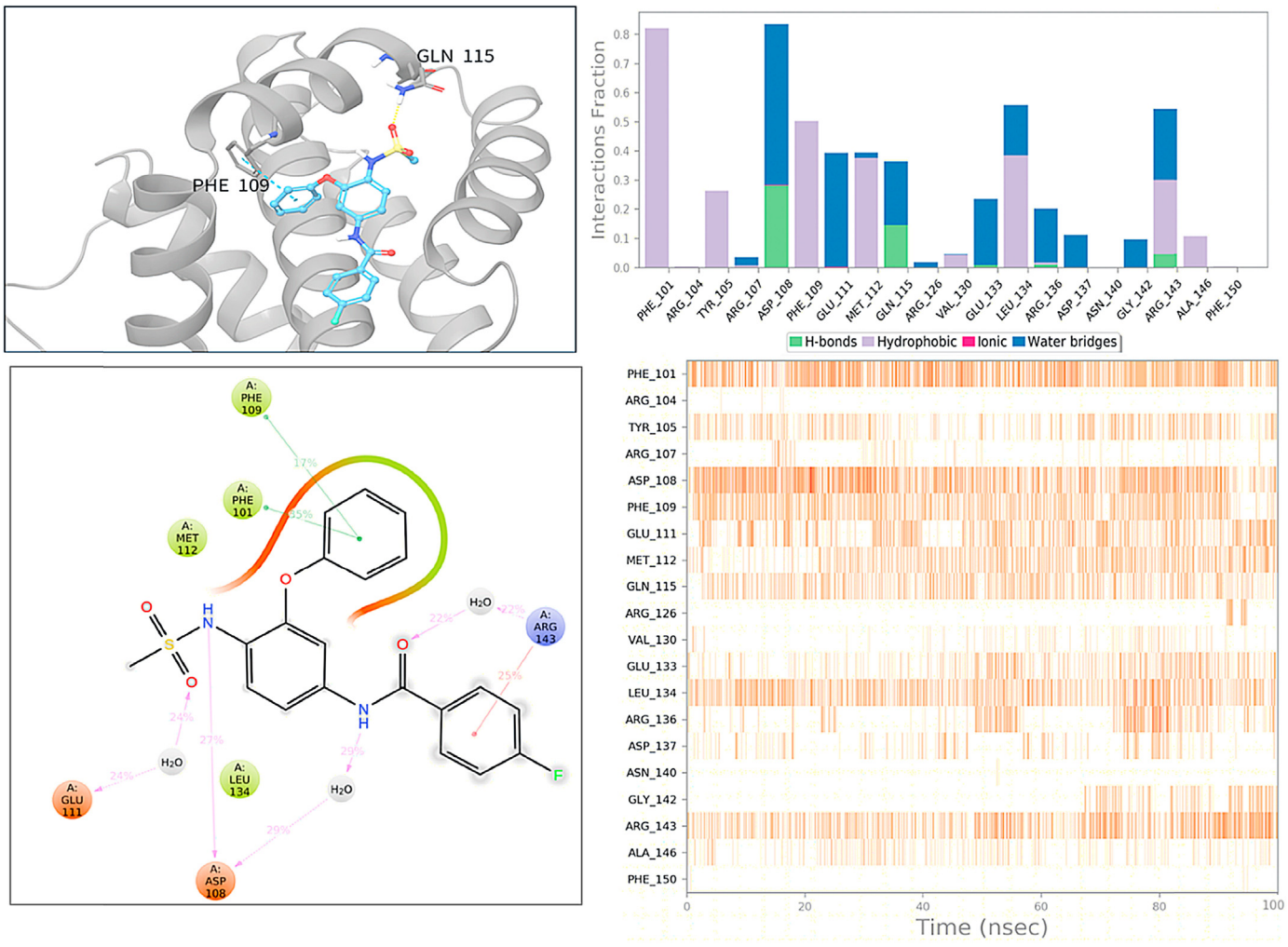

Fig. 9. 2D and 3D ligand interactions diagrams, interaction fractions and contact map of **N17** at the binding pocket residues of BCL-2.

Table 5
Average MM/GBSA free energy values of the studied compounds at the human COX-1, COX-2 and BCL-2 protein targets during the MD simulations.

Target	Compound	Average MM/GBSA score (kcal/mol)
COX -1	N2	−71.02
COX-1	N10	−52.84
COX-1	N13	−58.59
COX-1	N16	−59.05
COX-2	N2	−60.27
COX-2	N6	−66.88
COX-2	N7	−58.65
COX-2	N8	−65.33
COX-2	N9	−69.22
COX-2	N10	−46.58
COX-2	N13	−72.83
COX-2	N15	−67.96
COX-2	N17	−74.37
BCL-2	N8	−48.07
BCL-2	N10	−50.24
BCL-2	N13	−68.43
BCL-2	N17	−66.53

tested compounds only **N17** exhibited a good potency, which is closer to widely used chemotherapeutic agent doxorubicin, in colon and breast cancer cells with no observed toxicity in healthy cells at the highest tested concentration (200 μM). The mechanism of action studies, as well as docking and MD simulations provided partial evidence for the apoptotic cell death and possible involvement of BAX/BCL-2directed pathway. Besides, the results of docking and MD simulation studies elucidated the reasons for the selectivity of the synthesized compounds against COX enzymes. Overall, all synthesized compounds obey the druggability rules and can be promising drug candidates for future developments due to their acceptable ADME profiles and drug-likeness properties. Based on the findings in this study, it could be hypothesized that amide and sulfonamide derivatives of nimesulide may confer a new approach to obtain more potent and safer candidates for NSAIDs.

4. Experimental

4.1. Chemistry

All chemicals were supplied from commercial sources and used directly unless otherwise stated. Melting points were recorded on a X-4 melting-point apparatus and uncorrected. Thin-layer chromatography was performed using precoated Kieselgel $60GF_{254}$ (Merck) plates. The visualization of the spots was done by 254 nm UV light. Column chromatography technique was applied for purification of products using silica gel 60 (230–400 mesh, Merck). PerkinElmer Spectrum 100 FTIR spectrophotometer was used to record infrared spectra with ATR apparatus. ^{1}H and ^{13}C spectra were

Table 6
Average MM/GBSA free energy values of the reference molecules against COX-1, COX-2, and BCL-2 targets during the MD simulations.

MM/GBSA Scores of Reference Molecules (kcal/mol)		
COX-1	Celecoxib	−72.58
COX-2	Rofecoxib	−65.56
	Nimesulide	−53.62
BCL-2	Venetoclax	−81.85
	Nimesulide	−36.39

Table 7
Therapeutic activity predictions of studied compounds by the Inflammation-QSAR models.

Compound	Inflammation-QSAR[a]
N1	0.38
N2	0.40
N3	0.46
N4	0.41
N5	0.30
N6	0.34
N7	0.34
N8	0.40
N9	0.39
N10	0.66
N11	0.40
N12	0.58
N13	0.54
N14	0.67
N15	0.45
N16	0.68
N17	0.65

[a] Potential anti-inflammatory activity. Cutoff is 0.5. Values higher than 0.5 indicate potentially active compounds. Training set consists of approved drugs. Model description: Training set N = 598, Test set N = 93, Sensitivity = 0.86, Specificity = 0.84, Accuracy = 0.85, MCC = 0.69. Reference: Clarivate Analytics.

Table 8
Therapeutic activity predictions of studied compounds by the Cancer- QSAR models.

Compound	Cancer-QSAR[a]
N1	0.36
N2	0.36
N3	0.32
N4	0.45
N5	0.46
N6	0.54
N7	0.54
N8	0.54
N9	0.56
N10	0.44
N11	0.43
N12	0.51
N13	0.56
N14	0.62
N15	0.60
N16	0.29
N17	0.45

[a] Potential activity against cancer. Cutoff is 0.5. Values higher than 0.5 indicate potentially active compounds. Training set consists of approved drugs. Model description: Training set N = 886, Test set N = 167, Sensitivity = 0.89, Specificity = 0.83, Accuracy = 0.86, MCC = 0.72. Reference: Clarivate Analytics.

collected on 400/100 MHz Jeol and 600/150 MHz Agilent High-Performance Digital FT-NMR spectrometers using DMSO-d_6 as solvent. Splitting patterns are reported as follows: s, singlet; d, doublet; t, triplet; q, quartet; sept, septet; m, multiplet; dd, double doublet; dt, double triplet; td, triple doublet and ddd, doublet of doublet of doublets. The molecular weights of products were detected by Shimadzu LC-MS/MS 8040 Liquid Chromatograph Mass Spectrometer with an ESI source. The purity of compounds (>95%) was confirmed by the Shimadzu Prominence LC-20A Semi-Preparative HPLC system with a PDA detector and Shim-pack ODS(H) 250 × 4.6 mm, 5 μm C18 column. The gradient program was set 20% H_2O (B) in methanol (A) was used from 0 to 5 min, 20–60% B from 5 to 30 min, 60% B from 30 to 35 min, 60-20% B from 35 to 40 min and 20% B from 40 to 45 min with a flow rate 1.0 mL/min. Literature search of compounds was done using Reaxys database.

4.1.1. General procedure a for the synthesis of N1–N4, N6–N11 and N14–N17

N-(4-Amino-2-alkoxyphenyl)methanesulfonamide derivative was dissolved in enough chloroform. Triethylamine (Et_3N) and substituted benzoyl chloride or substituted benzenesulfonyl chloride were added dropwise to the solution in an ice bath. The mixture was stirred at room temperature for various reaction times. After completion of the reaction detected by TLC (hexane:ethyl acetate), the mixture was poured into ice-water and extracted with $CHCl_3$ (3 times). The combined organic layer was washed with 10% HCl and water, respectively, dried over anhydrous Na_2SO_4 and concentrated in vacuo. The crude product was purified using crystallization or column chromatography techniques.

4.1.1.1. N-(3-Ethoxy-4-(methylsulfonamido)phenyl)-2-nitrobenzamide (N1). The reaction was performed under general procedure A conditions using *N*-(4-amino-2-ethoxyphenyl)methanesulfonamide (0.217 mmol; 50 mg), 2-nitrobenzoyl chloride (0.26 mmol; 48.3 mg; 34.4 μL; 1.2 equiv.) and Et_3N (0.26 mmol; 26.4 mg; 36.3 μL; 1.2 equiv.) with 2.5 h reaction time. The crude product was purified by crystallization with ethyl alcohol to give compound **N1**. Cream-colored solid; 54 mg; 65% yield; m.p.149–151 °C; R_f = 0.28 (hexane:ethyl acetate, 1:1); IR (ATR) ϑ 3308, 3258, 3113, 3080, 3024, 2986, 2937, 2879, 1655, 1608, 1509, 1475, 1420, 1331, 1315, 1257, 1147, 964 cm^{-1}; ^1H NMR (400 MHz, DMSO-d_6, ppm): δ 10.67 (s, 1H), 8.79 (s, 1H), 8.11 (dd, J = 8.5 and 1.3 Hz, 1H), 7.84 (td, J = 7.8 and 1.0 Hz, 1H), 7.72–7.74 (m, 2H), 7.45 (d, *J* = 2.0 Hz, 1H), 7.11–7.17 (dd and t, J = 8.6, 2.6 and 8.6 Hz, 2H), 4.01 (q, *J* = 6.9 Hz, 2H), 2.88 (s, 3H), 1.35 (t, *J* = 6.9 Hz, 3H); ^{13}C NMR (100 MHz, DMSO-d_6, ppm): 164.6, 153.1, 146.9, 138.6, 134.6, 133.1, 131.6, 129.8, 128.2, 124.8, 121.8, 111.9, 104.6, 64.3, 40.6, 15.1; LC/MS (ESI) *m/z*: 378.0 $[M - H]^-$; HPLC analysis, t_R = 3.47 min, 99.66% purity.

4.1.1.2. N-(3-Ethoxy-4-(methylsulfonamido)phenyl)-3-nitrobenzamide (N2). The reaction was performed under general procedure A conditions using *N*-(4-amino-2-ethoxyphenyl) methanesulfonamide (0.217 mmol; 50 mg), 3-nitrobenzoyl chloride (0.26 mmol; 48.3 mg; 1.2 equiv.) and Et_3N (0.26 mmol; 26.4 mg; 36.3 μL; 1.2 equiv.) with 3 h reaction time. The crude product was

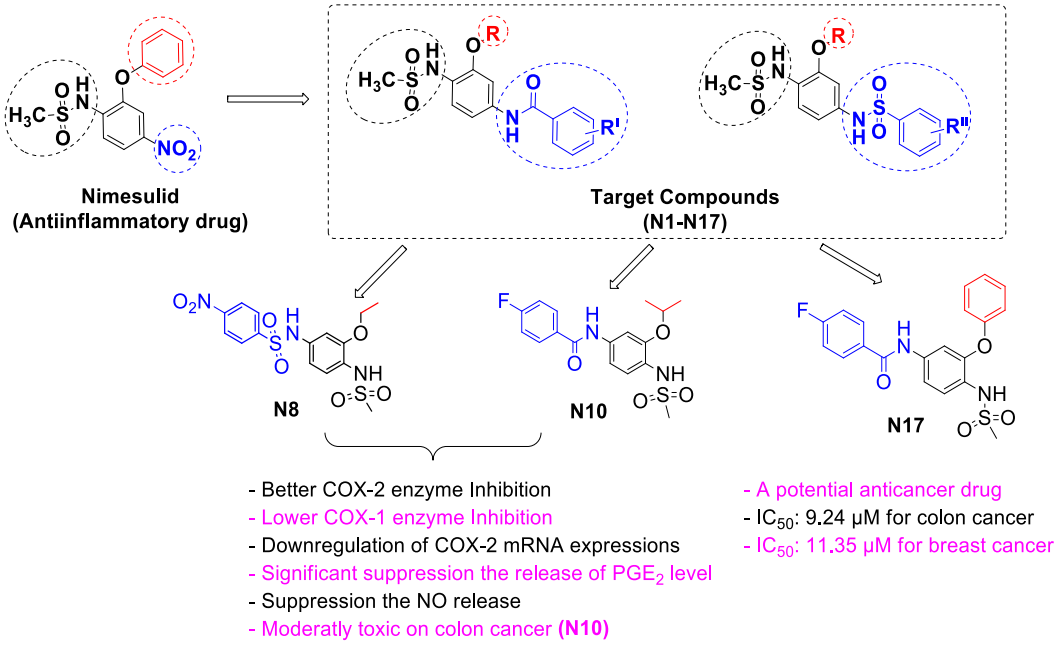

Fig. 10. An overview of biological data of potent nimesulide derivatives.

purified by crystallization with ethyl alcohol to give compound **N2**. White solid; 54 mg; 65% yield; m.p.177–179 °C; R_f = 0.43 (hexane:ethyl acetate, 1:1); IR (ATR) ϑ 3349, 3243, 3088, 2983, 2939, 1658, 1610, 1533, 1475, 1335, 1320, 1272, 1156, 972 cm^{-1}; ^1H NMR (400 MHz, DMSO-d_6, ppm): δ 10.56 (s, 1H), 8.81 (s, 1H), 8.75 (t, *J* = 1.9 Hz, 1H), 8.41 (ddd, J = 8.2, 2.2 and 0.8 Hz, 1H), 8.36 (dt, J = 7.9 and 1.4 Hz, 1H), 7.81 (t, *J* = 7.9 Hz, 1H), 7.55 (d, *J* = 2.1 Hz, 1H), 7.32 (dd, J = 8.5 and 2.1 Hz, 1H), 7.18 (d, *J* = 8.5 Hz, 1H), 4.1 (q, *J* = 7.0 Hz, 2H), 2.89 (s, 3H), 1.36 (t, *J* = 6.9 Hz, 3H); ^{13}C NMR (100 MHz, DMSO-d_6, ppm): 163.8, 152.9, 148.3, 138.3, 136.7, 134.7, 130.8, 127.8, 126.8, 122.9, 122.0, 112.8, 105.6, 64.4, 40.7, 15.1; LC/MS (ESI) *m/z*: 378.0 [M − H]$^-$; HPLC analysis, t_R = 3.62 min, 98.48% purity.

4.1.1.3. N-(3-Ethoxy-4-(methylsulfonamido)phenyl)-4-nitrobenzamide (N3). The reaction was performed under general procedure A conditions using *N*-(4-amino-2-ethoxyphenyl)methanesulfonamide (0.217 mmol; 50 mg), 4-nitrobenzoyl chloride (0.26 mmol; 48.3 mg; 1.2 equiv.) and Et_3N (0.26 mmol; 26.4 mg; 36.3 μL; 1.2 equiv.) with 2 h reaction time. The crude product was purified by washing with hot ethyl alcohol to give compound **N3**. Yellow solid; 58 mg; 71% yield; m.p.242–244 °C; R_f = 0.50 (hexane:ethyl acetate, 1:1); IR (ATR) ϑ 3393, 3267, 3111, 3068, 3017, 2973–2862, 1682, 1605, 1557, 1515, 1478, 1413, 1388, 1325, 1258, 1155, 975 cm^{-1}; ^1H NMR (600 MHz, DMSO-d_6, ppm): δ 10.55 (s, 1H), 8.79 (s, 1H), 8.36 (d, *J* = 8.5 Hz, 2H), 8.16 (d, *J* = 8.3 Hz, 2H), 7.58 (s, 1H), 7.32 (d, *J* = 8.2 Hz, 1H), 7.20 (d, *J* = 8.4 Hz, 1H), 4.06 (q, 2H), 2.92 (s, 3H), 1.39 (t, 3H); ^{13}C NMR (150 MHz, DMSO-d_6, ppm): 164.3, 152.7, 149.6, 141.0, 138.2, 129.6, 127.6, 124.0, 122.0, 112.7, 105.5, 64.3, 40.6, 15.0; LC/MS (ESI) *m/z*: 378.0 [M − H]$^-$; HPLC analysis, t_R = 7.83 min, 99.56% purity.

4.1.1.4. N-(3-Isopropoxy-4-(methylsulfonamido)phenyl)-4-nitrobenzamide (N4). The reaction was performed under general procedure A conditions using *N*-(4-amino-2-isopropoxyphenyl) methanesulfonamide (0.205 mmol; 50 mg), 4-nitrobenzoyl chloride (0.246 mmol; 45.6 mg; 1.2 equiv.) and Et_3N (0.246 mmol; 24.9 mg; 34.3 μL; 1.2 equiv.) with 2.5 h reaction time. The crude product was purified by washing with cold diethyl ether to give compound **N4**. Yellow-green solid; 59 mg; 73% yield; m.p.214–217 °C; R_f = 0.63 (hexane:ethyl acetate, 1:1); IR (ATR) ϑ 3394, 3277, 3108, 3082, 3060, 3016, 2979, 2931, 2864, 1680, 1602, 1510, 1416, 1400, 1346, 1323, 1264, 1155, 979 cm^{-1}; ^1H NMR (600 MHz, DMSO-d_6, ppm): δ 10.52 (s, 1H), 8.69 (s, 1H), 8.35 (d, *J* = 7.6 Hz, 2H), 8.16 (d, *J* = 7.2 Hz, 2H), 7.58 (s, 1H), 7.31 (d, *J* = 8.1 Hz, 1H), 7.20 (d, *J* = 7.6 Hz, 1H), 4.57 (m, 1H), 2.91 (s, 3H), 1.33 (s, 6H); ^{13}C NMR (150 MHz, DMSO-d_6, ppm): 164.3, 151.5, 149.6, 141.0, 138.1, 129.6, 127.7, 124.0, 122.5, 112.5, 106.4, 70.6, 40.6, 22.1; LC/MS (ESI) *m/z*: 392.0 [M − H]$^-$; HPLC analysis, t_R = 26.54 min, 98.15% purity.

4.1.1.5. N-(3-Ethoxy-4-(methylsulfonamido)phenyl)-2-nitrobenzenesulfonamide (N6). The reaction was performed under general procedure A conditions using *N*-(4-amino-2-ethoxyphenyl) methanesulfonamide (0.217 mmol; 50 mg), 2-nitrobenzenesulfonyl chloride (0.26 mmol; 57.7 mg; 1.2 equiv.) and Et_3N (0.26 mmol; 26.4 mg; 36.3 μL; 1.2 equiv.) with 12 h reaction time. The crude product was purified by column chromatography (silica gel) with hexane:ethyl acetate (2:1) to give compound **N6**. White solid; 67 mg; 75% yield; m.p.174–178 °C; R_f = 0.43 (hexane:ethyl acetate, 1:1); IR (ATR) ϑ 3264, 3106, 3023, 2982, 2938, 2887, 1611, 1539, 1483, 1409, 1360, 1333, 1154, 1122, 916 cm^{-1}; ^1H NMR (400 MHz, DMSO-d_6, ppm): δ 10.71 (s, 1H), 8.76 (s, 1H), 7.92–7.96 (m, 2H), 7.76–7.83 (m, 2H), 7.05 (d, *J* = 8.5 Hz, 1H), 6.75 (d, *J* = 2.3 Hz, 1H), 6.59 (dd, J = 8.5 and 2.3 Hz, 1H), 3.92 (q, *J* = 6.9 Hz, 2H), 2.83 (s, 3H), 1.28 (t, *J* = 6.9 Hz, 3H); ^{13}C NMR (100 MHz, DMSO-d_6, ppm): 153.1, 148.5, 136.0, 135.3, 133.1, 131.7, 130.5, 128.1, 125.1, 122.8, 112.7, 105.4, 64.3, 40.8, 14.8; LC/MS (ESI) *m/z*: 414.0 [M − H]$^-$; HPLC analysis, t_R = 3.33 min, 98.07% purity.

4.1.1.6. N-(3-Ethoxy-4-(methylsulfonamido)phenyl)-3-nitrobenzenesulfonamide (N7). The reaction was performed under general procedure A conditions using *N*-(4-amino-2-ethoxyphenyl) methanesulfonamide (0.217 mmol; 50 mg), 3-nitrobenzenesulfonyl chloride (0.26 mmol; 57.7 mg; 1.2 equiv.) and Et_3N (0.26 mmol; 26.4 mg; 36.3 μL; 1.2 equiv.) with 12 h reaction time. The crude product was purified by crystallization with ethyl alcohol to give compound **N7**. White solid; 70 mg; 78% yield; m.p.181–184 °C;

R_f = 0.43 (hexane:ethyl acetate, 1:1); IR (ATR) ϑ 3225, 3106, 3079, 3033, 2981–2878, 1612, 1526, 1487, 1405, 1351, 1343, 1297, 1151, 915 cm^{-1}; ^1H NMR (400 MHz, DMSO-d_6, ppm): δ 10.53 (s, 1H), 8.75 (s, 1H), 8.45 (t, *J* = 2.0 Hz, 1H), 8.415 (dd, J = 7.9 and 1.51 Hz, 1H), 8.12 (dt, J = 7.9 and 1.14 Hz, 1H), 7.83 (t, *J* = 8.0 Hz, 1H), 7.04 (d, *J* = 8.5 Hz, 1H), 6.75 (d, *J* = 2.3 Hz, 1H), 6.57 (dd, J = 8.5 and 2.3 Hz, 1H), 3.92 (q, *J* = 6.9 Hz, 2H), 2.83 (s, 3H), 1.27 (t, *J* = 6.9 Hz, 3H); ^{13}C NMR (100 MHz, DMSO-d_6, ppm): 153.1, 148.4, 141.3, 136.1, 133.2, 132.0, 128.2, 128.0, 123.0, 122.0, 113.0, 105.8, 64.4, 40.7, 14.8; LC/MS (ESI) *m/z*: 414.0 $[M - H]^-$; HPLC analysis, t_R = 22.80 min, 99.76% purity.

4.1.1.7. N-(3-Ethoxy-4-(methylsulfonamido)phenyl)-4-nitrobenzenesulfonamide (N8). The reaction was performed under general procedure A conditions using *N*-(4-amino-2-ethoxyphenyl) methanesulfonamide (0.217 mmol; 50 mg), 4-nitrobenzenesulfonyl chloride (0.26 mmol; 57.7 mg; 1.2 equiv.) and Et_3N (0.26 mmol; 26.4 mg; 36.3 μL; 1.2 equiv.) with 12 h reaction time. The crude product was purified by column chromatography (silica gel) with hexane:ethyl acetate (3:1) to give compound **N8**. White solid; 63 mg; 70% yield; m.p.199–200 °C; R_f = 0.50 (hexane:ethyl acetate, 1:1); IR (ATR) ϑ 3244, 3196, 3114, 3082, 3022, 2989, 2936, 2878, 1610, 1533, 1470, 1403, 1343, 1318, 1287, 1157, 982 cm^{-1}; ^1H NMR (400 MHz, DMSO-d_6, ppm): δ 10.59 (s, 1H), 8.75 (s, 1H), 8.34 (dt, J = 8.9 and 2.2 Hz, 2H), 7.97 (dt, J = 8.8 and 2.2 Hz, 2H), 7.03 (d, *J* = 8.5 Hz, 1H), 6.74 (d, *J* = 2.3 Hz, 1H), 6.57 (dd, J = 8.5 and 2.3 Hz, 1H), 3.92 (q, *J* = 6.9 Hz, 2H), 2.84 (s, 3H), 1.28 (t, *J* = 6.9 Hz, 3H); ^{13}C NMR (100 MHz, DMSO-d_6, ppm): 153.1, 150.4, 145.3, 136.3, 128.9, 128.1, 125.2, 122.8, 112.7, 105.5, 64.4, 40.8, 14.8; LC/MS (ESI) *m/z*: 414.0 $[M - H]^-$; HPLC analysis, t_R = 3.53 min, 99.63% purity.

4.1.1.8. N-(3-Isopropoxy-4-(methylsulfonamido)phenyl)-4-nitrobenzenesulfonamide (N9). The reaction was performed under general procedure A conditions using *N*-(4-amino-2-isopropoxyphenyl)methanesulfonamide (0.41 mmol; 0.1 g), 4-nitrobenzenesulfonyl chloride (0.62 mmol; 0.14 g; 1.5 equiv.) and Et_3N (0.62 mmol; 62.0 mg; 86.0 μL; 1.5 equiv.) with 24 h reaction time. The crude product was purified by column chromatography (silica gel) with hexane:ethyl acetate (2:1) to give compound **N9**. Cream-colored solid; 96 mg; 55% yield; m.p.204–207 °C; R_f = 0.63 (hexane:ethyl acetate, 1:1); IR (ATR) ϑ 3262, 3220, 3117, 3082, 2980, 2932, 2876, 1608, 1536, 1464, 1396, 1337, 1314, 1286, 1156, 858 cm^{-1}; ^1H NMR (600 MHz, DMSO-d_6, ppm): δ 10.58 (s, 1H), 8.70 (s, 1H), 8.37 (d, *J* = 8.4 Hz, 2H), 7.99 (d, *J* = 8.4 Hz, 2H), 7.07 (d, *J* = 8.5 Hz, 1H), 6.73 (s, 1H), 6.58 (d, *J* = 8.5 Hz, 1H), 4.43 (m, *J* = 6.0 Hz, 1H), 2.84 (s, 3H), 1.21 (d, *J* = 6.0 Hz, 6H); ^{13}C NMR (150 MHz, DMSO-d_6, ppm): 151.7, 150.3, 145.2, 135.9, 128.8, 128.1, 125.2, 123.4, 112.8, 106.6, 70.6, 40.7, 21.8; LC/MS (ESI) *m/z*: 428.0 $[M - H]^-$; HPLC analysis, t_R = 8.83 min, 99.49% purity.

4.1.1.9. N-(3-Isopropoxy-4-(methylsulfonamido)phenyl)-4-fluorobenzamide (N10). The reaction was performed under general procedure A conditions using *N*-(4-amino-2-isopropoxyphenyl) methanesulfonamide (0.205 mmol; 50 mg), 4-fluorobenzoyl chloride (0.245 mmol; 38.9 mg; 29.0 μL; 1.2 equiv.) and Et_3N (0.245 mmol; 24.8 mg; 34.2 μL; 1.2 equiv.) with 2 h reaction time. The crude product was purified by washing with cold diethyl ether to give compound **N10**. White solid; 60 mg; 81% yield; m.p.175–177 °C; R_f = 0.70 (hexane:ethyl acetate, 1:1); IR (ATR) ϑ 3338, 3247, 3081, 2986, 2936, 2910, 1651, 1603, 1505, 1420, 1385, 1328, 1273, 1156, 1110 cm^{-1}; ^1H NMR (600 MHz, DMSO-d_6, ppm): δ 10.22 (s, 1H), 8.66 (s, 1H), 8.01 (t, broad, 2H), 7.57 (s, 1H), 7.36 (t, *J* = 7.7 Hz, 2H), 7.28 (d, *J* = 8.2 Hz, 1H), 7.17 (d, *J* = 7.7 Hz, 1H), 4.565 (m, 1H), 2.90 (s, 3H), 1.33 (s, 6H); ^{13}C NMR (150 MHz, DMSO-d_6, ppm): 165.4 and 163.7 (d, J_{CF} = 249.11 Hz), 164.8, 151.5, 138.6, 131.73 and 131.72 (d, J_{CF} = 2.64 Hz), 130.82 and 130.76 (d, J_{CF} = 9.02 Hz), 127.8, 122.0, 115.9 and 115.7 (d, J_{CF} = 21.79 Hz), 112.4, 106.2, 70.6, 40.6, 22.1; LC/MS (ESI) *m/z*: 367.0 $[M + H]^+$; HPLC analysis, t_R = 4.29 min, 99.54% purity.

4.1.1.10. N-(3-Isopropoxy-4-(methylsulfonamido)phenyl)-4-methoxybenzamide (N11). The reaction was performed under general procedure A conditions using *N*-(4-amino-2-isopropoxyphenyl)methanesulfonamide (0.205 mmol; 50 mg), 4-methoxybenzoyl chloride (0.245 mmol; 41.9 mg; 33.3 μL; 1.2 equiv.) and Et_3N (0.245 mmol; 24.8 mg; 34.2 μL; 1.2 equiv.) with 2 h reaction time. The crude product was purified by washing with cold diethyl ether to give compound **N11**. Cream-colored solid; 58 mg; 75% yield; m.p.182–185 °C; R_f = 0.53 (hexane:ethyl acetate, 1:1); IR (ATR) ϑ 3345, 3242, 3057, 3024, 3006, 2981–2838, 1648, 1605, 1506, 1432, 1410, 1383, 1327, 1251, 1122, 1158 cm^{-1}; ^1H NMR (600 MHz, DMSO-d_6, ppm): δ 10.05 (s, 1H), 8.64 (s, 1H), 7.94 (d, *J* = 7.2 Hz, 2H), 7.59 (s, 1H), 7.29 (d, *J* = 8.2 Hz, 1H), 7.16 (d, *J* = 8.0 Hz, 1H), 7.04 (d, *J* = 7.2 Hz, 2H), 4.57 (m, 1H), 3.83 (s, 3H), 2.90 (s, 3H), 1.33 (s, 6H); ^{13}C NMR (150 MHz, DMSO-d_6, ppm): 165.3, 162.4, 151.5, 138.9, 130.0, 127.9, 127.3, 121.7, 114.1, 112.3, 106.1, 70.5, 55.9, 40.6, 22.1; LC/MS (ESI) *m/z*: 377.0 $[M - H]^-$; HPLC analysis, t_R = 25.04 min, 96.45% purity.

4.1.1.11. N-(3-Isopropoxy-4-(methylsulfonamido)phenyl)-4-fluorobenzenesulfonamide (N14). The reaction was performed under general procedure A conditions using *N*-(4-amino-2-isopropoxyphenyl)methanesulfonamide (0.205 mmol; 50 mg), 4-fluorobenzenesulfonyl chloride (0.245 mmol; 47.8 mg; 1.2 equiv.) and Et_3N (0.245 mmol; 24.8 mg; 34.2 μL; 1.2 equiv.) with 12 h reaction time. The crude product was purified by column chromatography (silica gel) with hexane:ethyl acetate (6:1) to give compound **N14**. White solid; 58 mg; 70% yield; m.p.172–174 °C; R_f = 0.65 (hexane:ethyl acetate, 1:1); IR (ATR) ϑ 3244, 3212, 3107, 3082, 2982, 2937, 2897, 1610, 1592, 1493, 1408, 1336, 1239, 1153, 1119 cm^{-1}; ^1H NMR (600 MHz, DMSO-d_6, ppm): δ 10.25 (s, 1H), 8.63 (s, 1H), 7.79 (q, J = 5.1 and 3.6 Hz, 2H), 7.39 (t, *J* = 8.8 Hz, 2H), 7.05 (d, *J* = 8.5 Hz, 1H), 6.71 (d, *J* = 2.1 Hz, 1H), 6.57 (dd, J = 8.5 and 2.2 Hz, 1H), 4.41 (sept, *J* = 6.0 Hz, 1H), 2.84 (s, 3H), 1.20 (d, *J* = 6.0 Hz, 6H); ^{13}C NMR (150 MHz, DMSO-d_6, ppm): 165.6 and 163.9 (d, J_{CF} = 251.6 Hz), 151.7, 136.6, 136.18 and 136.16 (d, J_{CF} = 2.95 Hz), 130.23 and 130.16 (d, J_{CF} = 9.57 Hz), 128.1, 123.0, 117.0 and 116.9 (d, J_{CF} = 22.9 Hz), 112.6, 106.4, 70.6, 40.7, 21.8; LC/MS (ESI) *m/z*: 401.0 $[M - H]^-$; HPLC analysis, t_R = 23.06 min, 99.80% purity.

4.1.1.12. N-(3-Isopropoxy-4-(methylsulfonamido)phenyl)-4-methoxybenzenesulfonamide (N15). The reaction was performed under general procedure A conditions using *N*-(4-amino-2-isopropoxyphenyl)methanesulfonamide (0.205 mmol; 50 mg), 4-methoxybenzenesulfonyl chloride (0.245 mmol; 50.6 mg; 1.2 equiv.) and Et_3N (0.245 mmol; 24.8 mg; 34.2 μL; 1.2 equiv.) with 12 h reaction time. The crude product was purified by washing with cold diethyl ether to give compound **N15**. Cream-colored solid; 43 mg; 51% yield; m.p.182–184 °C; R_f = 0.45 (hexane:ethyl acetate, 1:1); IR (ATR) ϑ 3237, 3114, 3009, 2974–2849, 1610, 1595, 1498, 1472, 1328, 1262, 1121, 1153 cm^{-1}; ^1H NMR (600 MHz, DMSO-d_6, ppm): δ 10.09 (s, 1H), 8.60 (s, 1H), 7.67 (d, *J* = 7.5 Hz, 2H), 7.04 (m, 3H), 6.73 (s, 1H), 6.56 (d, *J* = 8.2 Hz, 1H), 4.40 (m, 1H), 3.77 (s, 3H), 2.84 (s, 3H), 1.21 (s, 6H); ^{13}C NMR (150 MHz, DMSO-d_6, ppm): 162.9, 151.7, 137.2, 131.5, 129.3, 128.2, 122.5, 114.9, 112.1, 105.9, 70.6, 56.1, 40.7, 21.8; LC/MS (ESI) *m/z*: 413.0 $[M - H]^-$; HPLC analysis, t_R = 22.15 min, 98.48% purity.

4.1.1.13. N-(3-Ethoxy-4-(methylsulfonamido)phenyl)-4-fluorobenzamide (N16). The reaction was performed under general procedure A conditions using *N*-(4-amino-2-ethoxyphenyl)

methanesulfonamide (0.51 mmol; 0.12 g), 4-fluorobenzoyl chloride (0.61 mmol; 97.0 mg; 1.2 equiv.) and Et_3N (0.61 mmol; 61.9 mg; 85.3 μL; 1.2 equiv.) with 3 h reaction time. The crude product was purified by washing with cold diethyl ether to give compound **N16**. Bright brown solid; 0.149 g; 83% yield; m.p.198−199 °C; $R_f = 0.53$ (hexane:ethyl acetate, 1:1); IR (ATR) ϑ 3336, 3259, 3106, 3066, 2995, 2983, 2944, 2905, 1645, 1603, 1509, 1413, 1333, 1235, 1155, 1123 cm^{-1}; ^1H NMR (400 MHz, DMSO-d_6, ppm): δ 10.24 (s, 1H), 8.77 (s, 1H), 8.00 (m, 2H), 7.57 (d, $J = 2.1$ Hz, 1H), 7.35 (t, $J = 8.9$ Hz, 2H), 7.29 (dd, J = 8.6 and 1.9 Hz, 1H), 7.16 (d, $J = 8.6$ Hz, 1H), 4.04 (q, $J = 6.9$ Hz, 2H), 2.89 (s, 3H), 1.36 (t, $J = 6.9$ Hz, 3H); ^{13}C NMR (100 MHz, DMSO-d_6, ppm): 165.9 and 163.4 (d, $J_{CF} = 249.04$ Hz), 164.9, 152.9, 138.8, 131.8, 130.9 and 130.8 (d, $J_{CF} = 8.92$ Hz), 127.9, 121.6, 116.1 and 115.8 (d, $J_{CF} = 28.13$ Hz), 112.1, 105.4, 64.3, 40.7, 15.1; LC/MS (ESI) *m/z*: 353.0 $[M + H]^+$; HPLC analysis, $t_R = 24.78$ min, 98.78% purity.

4.1.1.14. N-(3-Phenoxy-4-(methylsulfonamido)phenyl)-4-fluorobenzamide (N17). The reaction was performed under general procedure A conditions using *N*-(4-amino-2-phenoxyphenyl) methanesulfonamide (0.43 mmol; 0.12 g), 4-fluorobenzoyl chloride (0.52 mmol; 82.5 mg; 1.2 equiv.) and Et_3N (0.52 mmol; 52.6 mg; 72.5 μL; 1.2 equiv.) with 3 h reaction time. The crude product was purified by washing with cold diethyl ether to give compound **N17**. Cream-colored solid; 0.136 g; 79% yield; m.p.159−162 °C; $R_f = 0.73$ (hexane:ethyl acetate, 1:1); IR (ATR) ϑ 3336, 3240, 3083, 3061, 3029, 3012, 2934, 1651, 1603, 1588, 1506, 1488, 1399, 1324, 1200, 1157, 1115 cm^{-1}; ^1H NMR (400 MHz, DMSO-d_6, ppm): δ 10.25 (s, 1H), 9.23 (s, 1H), 7.93 (m, 2H), 7.52 (dd, J = 8.7 and 1.4 Hz, 1H), 7.42−7.28 (m, 3H+3H), 7.16 (m, 1H), 7.07 (m, 2H), 2.94 (s, 3H); ^{13}C NMR (100 MHz, DMSO-d_6, ppm): 165.9 and 163.4 (d, $J_{CF} = 249.3$ Hz), 164.9, 156.6, 151.3, 138.6, 131.6, 131.0 and 130.9 (d, $J_{CF} = 9.05$ Hz), 130.6, 128.0, 124.4, 123.7, 119.7, 115.9 and 115.73 (d, $J_{CF} = 22.0$ Hz), 115.69, 110.5, 40.9; LC/MS (ESI) *m/z*: 401.0 $[M + H]^+$; HPLC analysis, $t_R = 27.93$ min, 99.66% purity.

4.1.2. N-(3-Isopropoxy-4-(methylsulfonamido)phenyl)-4-methoxy-2-nitrobenzamide (N5)

N-(4-Amino-2-isopropoxyphenyl)methanesulfonamide (0.204 mmol; 50 mg) was dissolved in 3 mL DCM. 2-Nitro-4-methoxybenzoic acid (0.204 mmol; 40.2 mg), DCC (0.225 mmol; 46.4 mg; 1.1 equiv.) and DMAP (5.0 mg; 0.2 equiv.) were added to the solution in an ice bath. The mixture was refluxed for 16 h. After completion of the reaction detected by TLC (hexane:ethyl acetate), the mixture was poured into ice-water (10 mL) and extracted with ethyl acetate (3 × 10 mL). The combined organic layer was washed with water (20 mL), dried over anhydrous Na_2SO_4 and concentrated in vacuo. The crude product was purified by column chromatography (silica gel, hexane:ethyl acetate, 3:2). Light yellow solid; 60 mg; 69% yield; m.p.166−169 °C; $R_f = 0.33$ (hexane:ethyl acetate, 1:1); IR (ATR) ϑ 3319, 3246, 3154, 3114, 3068, 2980, 2931, 2850, 1657, 1613, 1506, 1421, 1342, 1318, 1275, 1162, 1115, 972 cm^{-1}; ^1H NMR (600 MHz, DMSO-d_6, ppm): δ 10.59 (s, 1H), 8.72 (s, 1H), 7.71 (d, $J = 8.5$ Hz, 1H), 7.60 (s, 1H), 7.47 (s, 1H), 7.38 (d, $J = 9.9$ Hz, 1H), 7.17 (d, $J = 8.5$ Hz, 1H), 7.13 (d, $J = 8.6$ Hz, 1H), 4.54 (m, $J = 5.9$ Hz, 1H), 3.89 (s, 3H), 2.89 (s, 3H), 1.31 (d, $J = 5.9$ Hz, 6H); ^{13}C NMR (150 MHz, DMSO-d_6, ppm): 164.1, 161.0, 157.0, 151.7, 148.9, 138.5, 131.1, 128.2, 124.8, 122.1, 119.2, 111.6, 109.9, 105.4, 70.6, 56.8, 40.6, 22.0; LC/MS (ESI) *m/z*: 422.0 $[M - H]^-$; HPLC analysis, $t_R = 6.92$ min, 99.91% purity.

4.1.3. General procedure B for the synthesis of N12 and N13

Terephthalamic acid (1.0 equiv.) was dissolved in enough DMF. EDCI.HCl (1.0 equiv.) and HOBt (1.0 equiv.) were added dropwise to the solution in an ice bath, respectively. The mixture was stirred in ice-bath for 30 min and room temperature for 1 h. Then, Et_3N (3.0 equiv.) and *N*-(4-amino-2-alkoxyphenyl)methanesulfonamide derivative (1.0 equiv.) were added, respectively. The mixture was heated at 100−120 °C for 24 h (comp. **N12**) and 43 h (comp. **N13**). After completion of the reaction detected by TLC (hexane:ethyl acetate), the mixture was cooled to room temperature and poured into ice-water. If there was precipitation, the solid was filtered and dried, if not, extraction with ethyl acetate (3 times) was performed. The combined organic layer was washed with $NaHCO_3$ solution and water, respectively, dried over anhydrous Na_2SO_4 and concentrated in vacuo. The crude products of **N12** and **N13** were purified by washing with cold diethyl ether and column chromatography (silica gel, hexane:ethyl acetate, 2:3) techniques, respectively.

4.1.3.1. N-(3-Isopropoxy-4-(methylsulfonamido)phenyl)terephthalamide (N12). The reaction was performed under general procedure B conditions as described above. Light brown solid; 24% yield; m.p.238−241 °C; $R_f = 0.20$ (hexane:ethyl acetate, 2:3); IR (ATR) ϑ 3447, 3396,3346, 3263, 3185, 2982, 2936, 2901, 1649, 1607, 1527, 1507, 1408, 1327, 1280, 1160 cm^{-1}; ^1H NMR (600 MHz, DMSO-d_6, ppm): δ 10.33 (s, 1H), 8.72 (s, 1H), 8.12 (s, 1H), 7.99 (s, 4H), 7.56 (d, 2H), 7.32 (d, $J = 8.6$ Hz, 1H), 7.18 (d, $J = 8.6$ Hz, 1H), 4.57 (m, $J = 6.0$ Hz, 1H), 2.89 (s, 3H), 1.33 (d, $J = 6.0$ Hz, 6H); ^{13}C NMR (150 MHz, DMSO-d_6, ppm): 167.5, 165.3, 151.5, 138.5, 137.5, 137.3, 128.0, 127.9, 122.1, 112.3, 106.1, 70.5, 40.6, 22.1; LC/MS (ESI) *m/z*: 390.0 $[M - H]^-$; HPLC analysis, $t_R = 20.72$ min, 98.96% purity.

4.1.3.2. N-(3-Phenoxy-4-(methylsulfonamido)phenyl)terephthalamide (N13). The reaction was performed under general procedure B conditions as described above. Cream-colored solid; 25% yield; m.p.228−231 °C (dec.); $R_f = 0.23$ (hexane:ethyl acetate, 2:3); IR (ATR) ϑ 3453, 3340, 3232, 3060, 3023, 2935, 2870, 2839, 1673, 1654, 1606, 1544, 1509, 1492, 1406, 1389, 1320, 1277, 1160 cm^{-1}; ^1H NMR (600 MHz, DMSO-d_6, ppm): δ 10.36 (s, 1H), 9.28 (s, 1H), 8.10 (s, 1H), 7.94 (m, J = 8.5 and 3.4 Hz, 4H), 7.55 (m, 2H), 7.42 (m, 3H), 7.36 (d, $J = 8.8$ Hz, 1H), 7.17 (t, $J = 7.3$ Hz, 1H), 7.08 (d, $J = 8.3$ Hz, 2H), 2.95 (s, 3H); ^{13}C NMR (150 MHz, DMSO-d_6, ppm): 167.6, 165.3, 156.4, 151.2, 138.4, 137.28, 137.27, 130.5, 128.0, 127.9, 127.8, 124.4, 123.7, 119.7, 115.6, 110.4, 40.8; LC/MS (ESI) *m/z*: 424.0 $[M - H]^-$; HPLC analysis, $t_R = 18.47$ min, 98.30% purity.

4.2. Biological evaluation

4.2.1. Screening of cyclooxygenase Inhibitory

The inhibitory activity of the new compounds on human recombinant COX-1 and COX-2 were examined by following the instructions given for the COX (human) Inhibitor Screening Assay Kit (Cayman Chemical). The assay kit provides the quantification of prostanoid products as a yield of the COX reaction. Briefly, the purified COX-2 enzyme was pre-incubated with the compounds at 1 μM for 10 min at 37 °C. The COX reaction was initiated by adding arachidonic acid as a substrate at 100 μM and 30 s later stannous chloride solution was used to stop enzyme catalysis. The compounds showing an inhibitory effect for the COX-2 enzyme were also screened on COX-1 at 10 μM with the same experimental process. Inhibitory activity of each compound was determined in two independent experiments, in triplicate. As positive controls, nimesulide and celecoxib were used in this assay.

4.2.2. Cell culture

For the inflammation studies, human monocyte THP-1 cells were cultured in the RPMI-1640 medium supplemented with 100 U/mL penicillin, 100 μg/mL streptomycin, and 10% fetal bovine serum (FBS). When the concentration of suspension culture reached enough point, the cells were plated at a density of

1×10^6 cells/mL in 6 well plates and treated with 10 ng/mL of PMA to differentiate the monocyte into macrophage for 24 h. For the resting stage, cells were maintained in PMA-free fresh medium for another 24 h under the same culturing condition before treatment. RAW264.7 was maintained in high glucose Dulbecco's modified Eagle medium (DMEM) containing 10% FBS, 100 U/mL penicillin, and 100 μg/mL streptomycin. The cell lines HT-29 (human colon cancer cells), PC-3 (human prostate cancer cells), MCF-7 (human breast cancer cells), and HUVEC (human healthy umbilical cells) were routinely propagated in the identical medium of the murine macrophage cell line for the screening of anticancer effects of compounds. All cells were incubated in a humidified atmosphere at 37 °C and 5% CO_2. For all the treatment processes, compounds were dissolved in DMSO and maximum DMSO content in wells did not exceed 1.0%.

4.2.2.1. Determination of LPS-Induced PGE_2 release. The effect of compounds on the release of PGE_2 in medium were investigated according to the manufacturer's instructions of Thermo Fisher invitrogen PGE_2 ELISA Kit (EHPGE2). Differentiated THP-1 cells were treated with compounds at 50 μM doses and simultaneously stimulated with 1 μg/mL of LPS. After 24 h incubation, supernatants were collected for the ELISA process and the total protein content of viable cells was quantified with Thermo Fisher Pierce BCA Protein Assay Kit for normalization.

4.2.2.2. Quantification of NO release. The concentration of released NO in media was quantified by using the Griess reaction method as previously described [45]. Basically, RAW264.7 macrophage was plated to a 24-well plate at 4×10^5 cells/mL density in phenol-free media and left for 24 h incubation. Then, cells were treated with compounds at 20 and 50 μM doses and simultaneously stimulated with LPS (1 μg/mL) for 24 h. At the end of the incubation, supernatants were collected for the quantification of NO concentration and the total protein content of viable cells were quantified with BCA assay for normalization. 20 μM of 1400 W was used as a positive control.

4.2.2.3. MTT & sulforhodamine B (SRB) cell cytotoxicity assays. The cytotoxicity of NDs was determined by MTT assay. Briefly, cancer and healthy cell lines, in the exponential growth phase, were plated in 96-well plate at 5×10^4 cells/mL (100 μL per well). After 24 h of incubation at 37 °C, cells were treated with compounds at 100 μM doses for 48 h. At the end of the incubation period, MTT solution was added to each well at 1 mg/mL final concentration for 2 h. Cell medium was aspirated from each well and precipitated formazan crystal was dissolved in dimethyl sulfoxide and the absorbance was read at 570 and for background subtraction at 620 nm by using a microplate reader (Tecan Infinite® 200 PRO, Switzerland).

To determine the IC_{50} value of compounds, a slightly modified SRB assay, which is addressed to Vanicha&Kanyawim, was performed in each cell line [46]. Briefly, cells were seeded in 96-well plate at 5×10^4 cells/mL (100 μL per well) for SRB assay. The cells were left at 37 °C for 24 h incubation in their exponential growth phase then treated with compounds (0–200 μM) for 48 h. After the treatment period, supernatant from each well was aspirated carefully and cells were fixed with 10% (m/V) trichloroacetic acid (TCA) solution at 4 °C for 1 h. At the end of the fixation step, TCA solution was removed and washed with distilled water five times. Then the plate was left for air-drying at room temperature. When plates were completely dried, 100 μL of 0.04 (m/V) SRB solution was added to each well for 30 min at room temperature. To remove the unbound dye, the plate was rinsed in 1% (V/V) acetic acid solution four times. 200 μL of 10 mM of Tris base solution (pH:10.5) was added to wells to solubilize the protein-bound dye on the gyratory shaker for 10 min. The absorbance was determined by using a microplate reader (Tecan Infinite® 200 PRO, Switzerland) at 565 nm. IC_{50} values of compounds for each cell line were evaluated by GraphPad Prism 5 software. In both assays, doxorubicin was used as a positive control.

4.2.2.4. Gene expression analyses by quantitative PCR. The mRNA expression levels of COX-1, COX-2, iNOS, TNF-α, IL-1β and as housekeeping gene β-Actin were quantified by using specific TaqMan® probes (Thermo Scientific, Rockford, IL, USA). The total RNA content was isolated from THP-1 cells for the analysis of COX genes; and RAW 264.7 cell lines for other pro-inflammatory genes. Isolation was taken place by using a commercially available Pure Link® RNA mini kit with slight modification and a high-capacity cDNA reverse transcription kit (Applied Biosystems, Foster City, CA) was utilized for cDNA synthesis as described in previous studies [17,45]. In the presence of cDNA samples and TaqMan® probes, real-time PCR amplifications were recorded by Applied Biosystems 7500 Real Time PCR Systems (Applied Biosystems, Thermo Fisher Scientific). The comparative ΔΔCt method was implemented to determine the change in the mRNA levels.

4.2.3. Immunoblotting assay

The effects of **N17** on protein expression levels of BAX and BCL-2 were assigned by western blotting as previously described [45]. Briefly, MCF-7 cells were seeded at 6-well plates with a density 1×10^6 cell/mL. The cells were incubated with the presence of test compounds for 24 h and total protein samples were isolated from cells by using RIPA buffer. The concentration of total protein lysates was determined by the BCA assay. Equally loaded samples were run throughout the discontinuous buffer system including 4% stacking and 12% separating gel [47]. By gel electrophoresis, proteins in the sample were forced to separate under an electrical current based on their sizes. The gel was subjected to Western blotting to be labelled with BAX, BCL-2, and β-actin primary antibodies (Santa Cruz Biotechnology, Santa Cruz, CA) at 4 °C. The non-binding primary antibody was removed by washing steps with TBST and the membrane was subjected to 2 h incubation with the recommended dilution of horseradish peroxidase (HRP) -conjugated secondary antibody. The substrate of HRP was supplied by the reagent named SuperSignal™ West Pico PLUS Chemiluminescent. The intensity of the chemiluminescence signal was scanned by the C-DiGit® Blot Scanner. The densitometric analysis was taken place by using Image Studio Digits Software 5.0 and the results were given as relative change.

4.2.4. Clonogenic assay

MCF-7 cells were seeded in 6-well plates at a concentration of 5×10^2 (1 mL/well) and left to attach for 24 h. After attachment, the medium was replaced, and the cells were treated with increasing concentrations of **N17** (25–100) in every 2 days for a total of 14 days. Next, cells were fixed in 1 mL of fixation solution (75% methanol and 25% acetic acid) for 30 min at room temperature. The fixation solution was taken away and wells were rinsed with dH_2O. The cells were stained with 1 mL of 0.5% crystal violet solution for 30 min at room temperature. Finally, wells were rinsed with dH_2O, photographed and colonies were counted using ImageJ Studio software.

4.2.5. SEM analyses for observation of apoptotic figures

The ultrastructural changes in colon cancer cells were detected by SEM analyses. Briefly, the cells were plated on coverslips in a 24-well culture plate and overnight incubated. Then, cells were treated with **N17** at 25 μM doses for 48 h. At the end of incubation, the cells

were washed with a PIPES buffer. The cell fixation was achieved in a 2.5% glutaraldehyde solution for 1 h at 4 °C. The fixed cells were maintained and dehydrated by a series of incubations in the ethanol bath (50-70-80-90-100-100%) for 7 min each. For the complete drying process, coverslips were subjected to HMDS for overnight incubation. In the last step, the slides were mounted on a metal stub and coated with conductive metal for the observing under FESEM (Zeiss Supra 40 VP).

4.3. Preparation of ligands N1–N17

The molecules (**N1**–**N17**) were sketched in Maestro [48] 2D Sketcher. 2D molecules were converted to 3D structures and prepared for docking simulations by LigPrep module of the Maestro [49] with OPLS3e force field [50] was used in the restrain minimization with heavy atom convergence of 0.3 Å. Epik was used in the determination of the protonation states at neutral pH for all molecules [51]. After ligand preparation, atomic ESP charges for all the ligand molecules were determined by Semi-empirical NDDO Module of Maestro [52]. PM3 method was used for semiempirical calculations. Partial charges obtained from PM3 optimization were used in docking.

4.4. Preparation of human COX proteins

Crystal structure of the human COX-1 (PDB ID: 6Y3C) and COX-2 structures (PDB ID: 5KIR) downloaded from Protein Data Bank [53–55]. The initial structures were simplified by removing 'B', C', and 'D' chains. Of the ligands present on the 'A' chain of the human COX-2 structure, only the co-crystallized ligand (Rofecoxib) was kept, and other ligands were removed. The used human COX-1 protein is crystallized in apo form. Therefore, another COX-1 protein crystallized from *Ovis aries* (PDB ID: 3KK6) [56] which includes the co-crystallized ligand (Celecoxib) at the binding pocket, was aligned with the 6Y3C-coded structure and ligand was merged to the binding pocket of the 6Y3C. As a result, human COX-1 protein containing the Celecoxib ligand, and human COX-2 protein containing the Rofecoxib ligand were prepared for docking studies. Protein preparations was performed by using Schrodinger's Maestro Molecular modeling package [48]. OPLS3e force field [50] was used in the restrain minimization with heavy atom convergence of 0.3 Å. Disulfide bonds were formed and missing side chains were fixed using Prime module [57]. Using PROPKA, protonation states were calculated according to physiological pH 7.4. BCL-2 protein, which was prepared as published in our previous study, was used [55].

4.5. Molecular docking and molecular dynamic simulations

All molecular docking studies were accomplished by using the Glide module of the Schrödinger Maestro 2018 software [39]. Standard precision was used. The top-docking poses of protein-ligand complex structures were located in simulation boxes and solvated with TIP3P water models. Partial charges were used. Counter ions and 0.15 M NaCl solution were added in order to neutralize the simulation systems. MD simulations were performed at Desmond [44]. TIP3P water models were used and OPLS3e force field was applied. Simulations conducted for 100 ns and 2000 frames with equal intervals during the simulations were recorded for each simulation. All simulations were performed at constant physiological temperature (310 K) and constant pressure (1.01325 bar) by creating isothermal-isobaric ensemble system with Nose–Hoover thermostat [58] and Martyna–Tobias–Klein barostat [59]. The average MM/GBSA binding free energy of the compounds were calculated using Prime.

4.6. Binary QSAR models

The MetaCore/MetaDrug platform of Clarivate Analytics was used for investigating the ADME features, toxicity predictions and therapeutic activities of the molecules. All molecules in the study were screened in 25 common diseases and 26 different toxicity QSAR models. The quality of binary QSAR models was validated using the sensitivity, specificity, accuracy and Matthews correlation coefficient (MCC) parameters.

4.7. Statistical analysis

Data are obtained by at least three independent biological replicates and expressed as ± standard error of the mean. The differences between treatment groups were assessed by the statistical technique called one-way ANOVA with Dunnett's post hoc test (*$p < 0.02$, **$p < 0.005$, ***$p < 0.001$).

Author contributions

The project was designed and supervised by T.B.T., M.A. and T.G. The studied compounds were designed by T.B.T., M.A. and T.G, synthesized and characterized by T.G and M.A. The bioactivity studies, data analysis, and construction of figures of the related parts were performed by A.O, Y.B.Y, and T.B.T. The draft of their relative sections was written by T.B.T, T.G and A.O. All the *in silico* simulations and molecular modeling studies were conducted by S.D and P.S. and corresponding sections were drafted by these authors. All authors contributed to the writing of article.

Declaration of competing interest

The authors declare that they have no known competing financial interests or personal relationships that could have appeared to influence the work reported in this paper.

Acknowledgement

This study was financially supported by a research grant from Scientific and Technological Research Council of Turkey (TUBITAK; Grant No. 117Z398) and partially Çanakkale Onsekiz Mart University (Scientific Research Projects, ID: FYL-2019-3123). Authors thank to Dr. Tuğba Taşkın Tok for contributions at the beginning of the TUBITAK project.

Appendix A. Supplementary data

Supplementary data to this article can be found online at https://doi.org/10.1016/j.ejmech.2021.113566.

Abbreviations Used

TLC	Thin-layer chromatography
UV	Ultraviolet
m.p.	Melting point
FT-IR	Fourier-transform infrared spectroscopy
ATR	Attenuated total reflection
^{1}H NMR	Proton nuclear magnetic resonance
^{13}C NMR	Carbon nuclear magnetic resonance
TMS	Tetramethylsilane
MS	Mass spectroscopy
DMSO	Dimethyl sulfoxide
DMF	Dimethylformamide
DCM	Dichloromethane
SAR	Structure-activity relationship

NSAIDs	Nonsteroidal anti-inflammatory drugs
PGs	Prostaglandins
COX	Cyclooxygenase
PGE_2	Prostaglandin E2
NO	Nitric oxide
NOS	Nitric oxide synthases
eNOS	Endothelial nitric oxide synthases
nNOS	Neuronal nitric oxide synthases
iNOS	Inducible nitric oxide synthase
IL-1β	Interleukin-1β
TNFα	Tumor necrosis factor-α
EMA	European Medicines Agency
PMA	Phorbol 12-myristate-13-acetate
NF-κB	Nuclear Factor kappa β
LPS	Lipopolysaccharide
MTT	3-(4,5-Dimethylthiazol-2-yl)-2,5-diphenyltetrazolium bromide
SRB	Sulforhodamine B
FDA	Food and Drug Administration
DOX	Doxorubicin
CEL	Celecoxib
RCX	Rofecoxib
MD	Molecular dynamics
MM-GBSA	Molecular Mechanics/Generalized Born Surface Area

References

[1] I. Bjarnason, C. Scarpignato, E. Holmgren, M. Olszewski, K.D. Rainsford, A. Lanas, Mechanisms of damage to the gastrointestinal tract from nonsteroidal anti-inflammatory drugs, Gastroenterology 154 (2018) 500–514.

[2] M.G. Perrone, D.D. Lofrumento, P. Vitale, F. De Nuccio, V. La Pesa, A. Panella, R. Calvello, A. Cianciulli, M.A. Panaro, A. Scilimati, Selective cyclooxygenase-1 inhibition by p6 and gastrotoxicity: preliminary investigation, Pharmacology 95 (2015) 22–28.

[3] A. Tanaka, H. Araki, Y. Komoike, S. Hase, K. Takeuchi, Inhibition of both COX-1 and COX-2 is required for development of gastric damage in response to nonsteroidal antiinflammatory drugs, J. Physiol. Paris 95 (2001) 21–27.

[4] K.D. Rainsford, Anti-inflammatory drugs in the 21st century, Inflammation in the Pathogenesis of Chronic Diseases 42 (2007) 3–27.

[5] T.D. Warner, F. Giuliano, I. Vojnovic, A. Bukasa, J.A. Mitchell, J.R. Vane, Nonsteroid drug selectivities for cyclo-oxygenase-1 rather than cyclo-oxygenase-2 are associated with human gastrointestinal toxicity: a full in vitro analysis, Proc. Natl. Acad. Sci. U.S.A. 96 (1999) 7563–7568.

[6] H. Suleyman, E. Cadirci, A. Albayrak, Z. Halici, Nimesulide is a selective COX-2 inhibitory, atypical non-steroidal anti-inflammatory drug, Curr. Med. Chem. 15 (2008) 278–283.

[7] S. Kayaalp, Medical Pharmacology, in Terms of Rational Treatment, Hacettepe-Tas Ltd. Sti, Ankara, 1998, pp. 123–125.

[8] H. Süleyman, K. Altinkaynak, F. Göçer, A. Maraş, F. Akçay, M.D. Onuk, A. Gepdiremen, Effect of nimesulide on the indomethacin- and ibuprofen-induced ulcer in rat gastric tissue, Pol. J. Pharmacol. 54 (2002) 255–259.

[9] I. Bjarnason, F. Bissoli, A. Conforti, L. Maiden, N. Moore, U. Moretti, K.D. Rainsford, K. Takeuchi, G.P. Velo, Adverse reactions and their mechanisms from nimesulide, in: K.D. Rainsford (Ed.), Nimesulide — Actions and Uses, Birkhäuser Basel, Basel, 2005, pp. 315–415.

[10] E.M. Agency, Commission Decision on This Article 31 Referral for Nimesulide Containing Medicinal Products, 2011.

[11] K.D. Rainsford, Nimesulide – a multifactorial approach to inflammation and pain: scientific and clinical consensus, Curr. Med. Res. Opin. 22 (2006) 1161–1170.

[12] E. Caiazzo, A. Ialenti, C. Cicala, The relatively selective cyclooxygenase-2 inhibitor nimesulide: what's going on? Eur. J. Pharmacol. 848 (2019) 105–111.

[13] M. Catarro, J.L. Serrano, S.S. Ramos, S. Silvestre, P. Almeida, Nimesulide analogues: from anti-inflammatory to antitumor agents, Bioorg. Chem. 88 (2019) 102966.

[14] S. Rasheed, S.S. Sánchez, S. Yousuf, S.M. Honoré, M.I. Choudhary, Drug repurposing: in-vitro anti-glycation properties of 18 common drugs, PloS One 13 (2018), e0190509.

[15] M. Scalise, C. Indiveri, Repurposing nimesulide, a potent inhibitor of the B0AT1 subunit of the SARS-CoV-2 receptor, as a therapeutic adjuvant of COVID-19, Slas Discovery: Adv. Sci. Drug Discov. 25 (2020) 1171–1173.

[16] S.S. Kulabas, F.C. Onder, Y.B. Yılmaz, A. Ozleyen, S. Durdagi, K. Sahin, M. Ay, T.B. Tumer, In vitro and in silico studies of nitrobenzamide derivatives as potential anti-neuroinflammatory agents, J. Biomol. Struct. Dyn. 38 (2020) 4655–4668.

[17] T.B. Tumer, F.C. Onder, H. Ipek, T. Gungor, S. Savranoglu, T.T. Tok, A. Celik, M. Ay, Biological evaluation and molecular docking studies of nitro benzamide derivatives with respect to in vitro anti-inflammatory activity, Int. Immunopharm. 43 (2017) 129–139.

[18] B. Su, E.S. Diaz-Cruz, S. Landini, R.W. Brueggemeier, Novel sulfonanilide analogues suppress aromatase expression and activity in breast cancer cells independent of COX-2 inhibition, J. Med. Chem. 49 (2006) 1413–1419.

[19] M. Wang, G. Lacy, M. Gao, K.D. Miller, G.W. Sledge, Q.H. Zheng, Synthesis of carbon-11 labeled sulfonanilide analogues as new potential PET agents for imaging of aromatase in breast cancer, Bioorg. Med. Chem. Lett 17 (2007) 332–336.

[20] T.A. Khattab, B.D.B. Tiu, S. Adas, S.D. Bunge, R.C. Advincula, pH triggered smart organogel from DCDHF-Hydrazone molecular switch, Dyes Pigments 130 (2016) 327–336.

[21] A.D. Snow, B.P. Nguyen, T. Lake, G.M. Castillo, M. Weigele, Substituted *N*-aryl benzamides and related compounds for treatment of amyloid diseases and synucleinopathies, their preparation and pharmaceutical compositions, WO (2005), 2005113489.

[22] S. Pericherla, J. Mareddy, G. Rani, D. P, P.V. Gollapudi, S. Pal, Chemical modifications of nimesulide, J. Braz. Chem. Soc. 18 (2007) 384–390.

[23] Y. Yamamoto, T. Hisa, J. Arai, Y. Saito, F. Yamamoto, T. Mukai, T. Ohshima, M. Maeda, Y. Ohkubo, Isomeric methoxy analogs of nimesulide for development of brain cyclooxygense-2 (COX-2)-targeted imaging agents: synthesis, in vitro COX-2-inhibitory potency, and cellular transport properties, Bioorg. Med. Chem. 23 (2015) 6807–6814.

[24] T.D. Warner, Introduction to "nimesulide: beyond COX-2, Clin. Exp. Rheumatol. 19 (2001) S1–S2.

[25] M.N. Khan, Y.S. Lee, Cyclooxygenase inhibitors: scope of their use and development in cancer chemotherapy, Med. Res. Rev. 31 (2011) 161–201.

[26] E. Ricciotti, G.A. FitzGerald, Prostaglandins and Inflammation, Arteriosclerosis, Thrombosis, and Vascular Biology 31 (2011) 986–1000.

[27] R. Nørregaard, T.H. Kwon, J. Frøkiær, Physiology and pathophysiology of cyclooxygenase-2 and prostaglandin E2 in the kidney, Kidney Research and Clinical Practice 34 (2015) 194–200.

[28] A. Bennett, in: J.R. Vane, R.M. Botting (Eds.), Nimesulide a Well Established Cyclooxygenase-2 Inhibitor with Many Other Pharmacological Properties Relevant to Inflammatory Diseases, Therapeutic Roles of COX-2 Inhibitors, vol. 524, 2001, p. 540.

[29] A. Bennett, G. Villa, Nimesulide: an NSAID that preferentially inhibits COX-2, and has various unique pharmacological activities, Expet Opin. Pharmacother. 1 (2000) 277–286.

[30] E. van den Bogaart, P.F. Mens, E.R. Adams, M.P. Grobusch, H. Schallig, Phagocytosis of hemozoin by RAW 264.7 cells, but not THP-1 cells, promotes infection by Leishmania donovani with a nitric oxide-independent mechanism, Parasitol. Int. 66 (2017) 196–206.

[31] S. Bertholet, E. Tzeng, E. Felley-Bosco, J. Mauël, Expression of the inducible NO synthase in human monocytic U937 cells allows high output nitric oxide production, J. Leukoc. Biol. 65 (1999) 50–58.

[32] A. Ozleyen, Y.B. Yilmaz, T.B. Tumer, Dataset on the differentiation of THP-1 monocytes to LPS inducible adherent macrophages and their capacity for NO/iNOS signaling, Data in Brief 35 (2021) 106786.

[33] T.J. Gross, K. Kremens, L.S. Powers, B. Brink, T. Knutson, F.E. Domann, R.A. Philibert, M.M. Milhem, M.M. Monick, Epigenetic silencing of the human NOS2 gene: rethinking the role of nitric oxide in human macrophage inflammatory responses, J. Immunol. 192 (2014) 2326–2338.

[34] R.G. Knowles, S. Moncada, Nitric oxide synthases in mammals, Biochem. J. 298 (Pt 2) (1994) 249–258.

[35] T.O. Fischmann, A. Hruza, X.D. Niu, J.D. Fossetta, C.A. Lunn, E. Dolphin, A.J. Prongay, P. Reichert, D.J. Lundell, S.K. Narula, P.C. Weber, Structural characterization of nitric oxide synthase isoforms reveals striking active-site conservation, Nat. Struct. Biol. 6 (1999) 233–242.

[36] B.R. Crane, R.J. Rosenfeld, A.S. Arvai, D.K. Ghosh, S. Ghosh, J.A. Tainer, D.J. Stuehr, E.D. Getzoff, N-terminal domain swapping and metal ion binding in nitric oxide synthase dimerization, EMBO J. 18 (1999) 6271–6281.

[37] S. Naureckiene, W. Edris, S.K. Ajit, A.H. Katz, K. Sreekumar, K.E. Rogers, J.D. Kennedy, P.G. Jones, Use of a murine cell line for identification of human nitric oxide synthase inhibitors, J. Pharmacol. Toxicol. Methods 55 (2007) 303–313.

[38] T.B. Tumer, B. Yılmaz, A. Ozleyen, B. Kurt, T.T. Tok, K.M. Taskin, S.S. Kulabas, GR24, a synthetic analog of Strigolactones, alleviates inflammation and promotes Nrf2 cytoprotective response: in vitro and in silico evidences, Comput. Biol. Chem. 76 (2018) 179–190.

[39] R.A. Friesner, R.B. Murphy, M.P. Repasky, L.L. Frye, J.R. Greenwood, T.A. Halgren, P.C. Sanschagrin, D.T. Mainz, Extra precision glide: docking and scoring incorporating a model of hydrophobic enclosure for protein-ligand complexes, J. Med. Chem. 49 (2006) 6177–6196.

[40] C. Michaux, C. Charlier, F. Julémont, X. de Leval, J.-M. Dogné, B. Pirotte, F. Durant, A new potential cyclooxygenase-2 inhibitor, pyridinic analogue of nimesulide, Eur. J. Med. Chem. 40 (2005) 1316–1324.

[41] K.J. Campbell, S.W.G. Tait, Targeting BCL-2 Regulated Apoptosis in Cancer, 2018, p. 8.

[42] A. Frenzel, F. Grespi, W. Chmelewskij, A. Villunger, Bcl2 family proteins in carcinogenesis and the treatment of cancer, Apoptosis 14 (2009) 584–596.

[43] G. Radha, S.C. Raghavan, BCL2: a promising cancer therapeutic target, Biochim. Biophys. Acta Rev. Canc 1868 (2017) 309–314.

[44] K.J. Bowers, E. Chow, H. Xu, R.O. Dror, M.P. Eastwood, B.A. Gregersen,

J.L. Klepeis, I. Kolossvary, M.A. Moraes, F.D. Sacerdoti, J.K. Salmon, Y. Shan, D.E. Shaw, Scalable algorithms for molecular dynamics simulations on commodity clusters, in: Proceedings of the 2006 ACM/IEEE Conference on Supercomputing, Association for Computing Machinery, Tampa, Florida, 2006, p. 84, es.
[45] D. Kapche, N.M. Lekane, S.S. Kulabas, H. Ipek, T.T. Tok, B.T. Ngadjui, I. Demirtas, T.B. Tumer, Aryl benzofuran derivatives from the stem bark of Calpocalyx dinklagei attenuate inflammation, Phytochemistry 141 (2017) 70–79.
[46] V. Vichai, K. Kirtikara, Sulforhodamine B colorimetric assay for cytotoxicity screening, Nat. Protoc. 1 (2006) 1112–1116.
[47] U.K. Laemmli, Cleavage of structural proteins during the assembly of the head of bacteriophage T4, Nature 227 (1970) 680–685.
[48] Maestro MolecularModelingPackage, 2018. New York.
[49] LigPrep, Schrodinger, LLC, New York, NY, 2018.
[50] K. Roos, C. Wu, W. Damm, M. Reboul, J.M. Stevenson, C. Lu, M.K. Dahlgren, S. Mondal, W. Chen, L. Wang, R. Abel, R.A. Friesner, E.D. Harder, OPLS3e: extending Force Field Coverage for Drug-Like Small Molecules, J. Chem. Theor. Comput. 15 (2019) 1863–1874.
[51] J.C. Shelley, A. Cholleti, L.L. Frye, J.R. Greenwood, M.R. Timlin, M. Uchimaya, Epik: a software program for pK(a) prediction and protonation state generation for drug-like molecules, J. Comput. Aided Mol. Des. 21 (2007) 681–691.
[52] Semi Empirical NDDO Protocol, LLC, New York, NY, 2018. Jaguar, Schrödinger.
[53] S.K. Burley, C. Bhikadiya, C. Bi, S. Bittrich, L. Chen, G.V. Crichlow, C.H. Christie, K. Dalenberg, L. Di Costanzo, J.M. Duarte, S. Dutta, Z. Feng, S. Ganesan, D.S. Goodsell, S. Ghosh, R.K. Green, V. Guranović, D. Guzenko, B.P. Hudson, C.L. Lawson, Y. Liang, R. Lowe, H. Namkoong, E. Peisach, I. Persikova, C. Randle, A. Rose, Y. Rose, A. Sali, J. Segura, M. Sekharan, C. Shao, Y.P. Tao, M. Voigt, J.D. Westbrook, J.Y. Young, C. Zardecki, M. Zhuravleva, RCSB Protein Data Bank: powerful new tools for exploring 3D structures of biological macromolecules for basic and applied research and education in fundamental biology, biomedicine, biotechnology, bioengineering and energy sciences, Nucleic Acids Res. 49 (2021) D437–D451.
[54] M. Miciaccia, B.D. Belviso, M. Iaselli, G. Cingolani, S. Ferorelli, M. Cappellari, P. Loguercio Polosa, M.G. Perrone, R. Caliandro, A. Scilimati, Three-dimensional structure of human cyclooxygenase (hCOX)-1, Sci. Rep. 11 (2021) 4312.
[55] B.J. Orlando, M.G. Malkowski, Crystal structure of rofecoxib bound to human cyclooxygenase-2, Acta crystallographica, Section F, Structural biology communications 72 (2016) 772–776.
[56] G. Rimon, R.S. Sidhu, D.A. Lauver, J.Y. Lee, N.P. Sharma, C. Yuan, R.A. Frieler, R.C. Trievel, B.R. Lucchesi, W.L. Smith, Coxibs interfere with the action of aspirin by binding tightly to one monomer of cyclooxygenase-1, Proc. Natl. Acad. Sci. U.S.A. 107 (2010) 28–33.
[57] M.P. Jacobson, D.L. Pincus, C.S. Rapp, T.J.F. Day, B. Honig, D.E. Shaw, R.A. Friesner, A hierarchical approach to all-atom protein loop prediction, Proteins: Structure, Function, and Bioinformatics 55 (2004) 351–367.
[58] W.G. Hoover, Canonical dynamics: equilibrium phase-space distributions, Phys. Rev. 31 (1985) 1695–1697.
[59] G.J. Martyna, D.J. Tobias, M.L. Klein, Constant pressure molecular dynamics algorithms, J. Chem. Phys. 101 (1994) 4177–4189.